QEEFoam: A Quasi-Eulerian-Eulerian model for polydisperse turbulent gas-liquid flows. Implementation in OpenFOAM, verification and validation

`QEEFoam`: a Quasi-Eulerian-Eulerian model for polydisperse turbulent gas-liquid flows. Implementation in OpenFOAM, verification and validation.

Dongyue Li[a,b], Yufeng Wei[c], Daniele Marchisio[d,*]

[a]*State Key Laboratory of Advanced Metallurgy, University of Science and Technology Beijing, Beijing, China*
[b]*DYFLUID Ltd, Beijing, China*
[c]*Department of Mathematics, Hong Kong University of Science and Technology, Hong Kong, China*
[d]*Politecnico di Torino, Torino, Italy*

Abstract

In this paper we present a new multiphase computational model for polydisperse turbulent gas-liquid flows. In this model the gas phase is transported by a single convection equation and the effect of turbulent dispersion is addressed by including a diffusion term. In order to close the system of equations, the gas phase velocity is calculated by employing the slip velocity concept or by solving an ODE. This procedure shares similarity with the Euler-Lagrange (E-L) method, in which the gas velocity is updated by bubble Lagrangian tracking, and with the Euler-Euler (E-E) method, and for this reason it is called the Quasi-Eulerian-Eulerian (Q-E-E) method. In order to account for polydispersity one single transport equation is added to describe the effects of bubble breakage and coalescence on the mean bubble size. The novel Q-E-E method was implemented in the open-source code OpenFOAM-7 and was used to simulate turbulent gas-liquid flows with three different geometries operating under different conditions. The predictions for the dynamical vortex structures, local phase fraction, global gas holdup, mean bubble size and vertical/horizontal liquid velocities were verified against the solution provided by the E-L solver or against published experimental data. Good agreement was found and with extremely small computational costs.

Keywords: Computational fluid dynamics, Bubbly flow, Eulerian-Eulerian model, OpenFOAM, Bubble column, Bubble size distribution

1. Introduction

Bubbly flows are omnipresent in engineering and are found in many applications, ranging from the chemical to the nuclear industry. For bubble-driven flows, the bubble movement is the main source of momentum for the flow field; these flows are often characterized by low liquid velocities and relatively high superficial gas velocities. The bubble-driven flow in ducts and columns with a small aspect ratio is usually complicated. Recirculating flow is quite common even at relatively low gas flow rates [40], which can speed up mass and heat transfer. If the gas superficial velocity is high, it leads to intense interaction between bubbles and bubble breakage and coalescence can be dominating. In vertical bubbly flows with a high aspect ratio, the small bubbles migrate to the wall resulting in a steeper velocity gradient in the near-wall region. On the opposite, the large bubbles migrate towards the center [87, 20]. The velocity profile resembles that of single phase flows. In all the cases, there

*Corresponding author. Tel: +39 0110904622. Fax: +39 0110904699. Email: daniele.marchisio@polito.it

is a strong coupling between the gas bubbles spatial distribution, the liquid velocity, the momentum exchange between gas and liquid and the resulting flow structure is quite complex.

Besides experimental investigations, bubbly flows can be also analyzed by using computational models, whose governing equations cannot be solved analytically except in very special cases. For process design and analysis, computational fluid dynamics (CFD) has become an important and indispensable tool. Specifically, the simulation methods for gas-liquid flows in CFD can be divided mainly into three categories. In the first category one finds multiphase direct numerical simulation methods (MP-DNS), based on the simple idea of directly tracking the interface between the involved phases. In the case of bubbly flows this implies tracking the evolution of the gas-liquid interface around each bubble. This is an extremely accurate method, but characterized by very high computational costs. These methods will not be discussed here, since they are usually restricted to very low Reynolds numbers and are suitable for dilute gas-liquid flows. Readers interested in the details are referred to the specialized literature [68].

In the Eulerian-Lagrangian (E-L) method [14, 39] the continuous phase is processed via the Eulerian framework, while the individual bubble motion is simulated through the solution of the corresponding Newton equation of motion. Bubble trajectories are calculated and by considering fixed control volumes the coupling with the continuous phase can be finalized. These discrete bubbles can be coarse-grained into larger bubble clusters to speed up the simulation and the bubble cluster is usually called parcels [79]. The E-L method features no numerical diffusion as the most important merit [10].

In the Eulerian-Eulerian (E-E) method [6, 63, 75, 21], both phases are evolved in the Eulerian framework and a different set of Navier-Stokes equations can be constructed for each phase. The coupling between these phases is achieved by the so-called momentum interfacial exchange term appearing in the momentum balance equations. In quadrature-based moments methods (QBMM) [58], the disperse phase is described by the generalized population balance equation while the continuous phase is controlled by the traditional Eulerian equations. Depending on the closure of the disperse phase velocity, this method can be easily extended to poly-disperse systems and bubble coalescence and breakage can be included. This method was investigated extensively in our previous works [48, 50, 49, 46]. Another promising method is the mixture model [57, 36] and one of its most popular implementations is based on the so-called algebraic slip model [80]. In the mixture model, instead of describing each phase by using its own continuity and momentum balance equation, only one continuity equation and one momentum balance equation are solved for the mixture of the two phases. All of these models except the E-L method do not keep track of the individual bubbles but represent an averaged description in which the space domain may contain a fraction of both the continuous and the disperse phases. Readers are suggested to other works for more information on the derivation and application of these mathematical models [35, 54, 83].

However, none of these methods is satisfactory. Recent efforts are going in the direction of coupling and linking different models but that requires the development of a common representational system for metadata that describe the employed computational tools, in order to make them interoperable at the semantic level [34]. The governing equations of the E-E method are quite complex, which implies that complicated numerical techniques are needed to handle the phase segregation problem and the phase coupling [65, 47]. Handling the numerical diffusion in the E-E method is also non-trivial, since high-order spatial discretization schemes usually generate boundedness problems, resulting in turn in catastrophic divergence [72]. The realizability of the moments in the E-QBMM cannot be easily ensured either and dozens of moment equations are needed to be solved for a three-dimensional test case. Meanwhile, fine meshes cannot be used in the traditional E-L method since the bubble size should be smaller than the cell size in order to calculate the momentum transfer between phases accurately [15]. Statistical noise cannot be avoided either. For a given desired accuracy, this greatly

increases the computational cost and a large number of numerical bubbles are required to eliminate statistical noise. For the mixture model, the boundary condition of the mixture velocity needs to be carefully treated and it is mainly used for gas-solid settling problems with very small slip velocity [1, 60].

Is it possible to have a computational model that simplifies the governing equations of the multiphase flow beyond these existing methods? The answer to this question seems to be yes. Sokolichin et al. [76] developed a simplified gas-liquid model from the two-phase E-E method. The spirit of this method is that, if one sums up the momentum equation of the gas and the liquid and neglects the terms involving the gas density ($\rho_g \ll \rho_l$), a liquid momentum equation without phase fraction is constructed. In this model, the governing equations fully correspond with the mass and momentum balance equations and the equation of state of a single-phase flow. Meanwhile, a phase fraction dependent acceleration term exists in the momentum equation. This term is used to describe a force which is directed upwards and is proportional to the local gas holdup. Therefore, the gas-liquid flow can be interpreted as a one-phase flow with an additional buoyancy source term in the momentum balance. However, this method is restricted to a very low local phase volume fractions. Ferry and Balachandar proposed a so-called fast or equilibrium Eulerian-Eulerian method for small particle response times τ [25, 26]. They express the particle velocity as an expansion in τ to remove the particle momentum partial differential equation. This equation is first-order accuracy with respect to τ but higher-order equations can also be derived. It was further extended to account near-wall approximation, which can accurately capture the high shear region behavior [27]. The very same approach was also used in other works to simulate particle-laden flows for small Stokes flows [74, 73]. Only the concentration field needs to be solved for particles of certain size range. Another possible similar simplification originates from the E-L method. If one replaces the Lagrangian particle equation with a gas phase convection equation under the Eulerian framework, the time consuming Lagrangian tracking is not necessary and the Lagrangian noise can be avoided. However, the equation system is not closed since the gas phase velocity is unknown. Therefore, the gas phase velocity needs to be modelled and a closed set of equation is finally obtained and can be solved.

The methods described so far are generally all solved assuming a monodisperse population of bubbles with constant and given size. However real bubbly flows are characterized by bubble breakage and coalescence, leading to polydispersity. Polydispersity not only exists in the field of chemical engineering, but also in other fields, such as oceanic breaking waves. However, the distribution function may have different shapes. In typical chemical engineering applications, namely bubble columns and bubbly flows confined in small pipes, many studies suggest that the bubbles size distribution follows a log-normal law [17, 67, 55]. Our previous study also employed the log-normal distribution for small droplets in stirred tanks [46]. In the field of the ocean wave, it was shown that the bubble size follows instead a power-law scaling [28, 22, 78, 8]. Among this, Garrett et al. [28] introduced the most widely used model, in which the air flow rate Q and turbulent dissipation rate $\bar{\varepsilon}$ are used to predict the bubble size distribution. It is shown that large bubbles smaller than the Hinze scale [33] are entrained. Such bubbles are stabilized by surface tension forces and do not fragment any further [22]. These small bubbles show a $-3/2$ power-law scaling with size. On the other hand, bubbles larger than the Hinze scale showed a $-10/3$ power law scaling. Many works claim that the Hinze scale is around 0.8 - 1 mm and that the power law is characterized by an exponents between 2.5 and 3.5. The reason for different exponents is due to different flow features and different bubble coalescence and breakage mechanisms. For example, Deane and Stokes [22], Loewen et al. [53] reported an exponent closer to 10/3. Some other studies showed that the exponent is closer to 3 [8, 70]. In order to investigate the bubble size distribution MP-DNS can be used. For example, in the work of Ahmed et al. [2], the front-tracking method has been used to investigate the effects of soluble surfactant and viscoelasticity on bubbly flows. On the contrary to this work, the bubble shape in their work can be

R3.2
R3.3

reconstructed with sharp interface and the turbulent related variables can be analysed. In the work of Soligo et al. [78], they employed the two-order-parameter phase-field method to describe droplets and surfactant dynamics. Similar with bubbles, the shape of droplets can be also reconstructed and investigated. They showed that the droplet size distribution also follows the $-10/3$ power law scaling. Wang et al. [84] employed 12 billion grid points to resolve bubbles/droplets in breaking waves by the volume of fluid method with a higher-order scheme. Their results shows a -1.46 and -3 power scaling for large bubbles, which is also closer to the theoretical values of Garrett et al. [28].

As previously mentioned, the MP-DNS is computationally very demanding and a cheaper alternative is to account for the bubble distribution by solving the population balance equation (PBE). Different methods were proposed to solve the PBE, such as the class method (CM) [42], the quadrature method of moments (QMOM) [59] and they were employed to reconstruct the bubble size distribution in many works [31, 86, 82, 71, 16, 29, 30, 12, 41]. However, these methods still require large computational resources [48, 46] and a even cheaper alternative could be the so-called one primary and one secondary particle method (OPOSPM) [24, 3, 4], which conserves only the total gas bubble number density and the total gas bubble volume density (i.e. volume fraction). In this method two transport equations for the total number density and the total volume fraction of the gas bubbles are solved together with a one-quadrature rule for closing the unclosed terms in the PBE. This method can be further simplified to a one-equation model for the solution of the PBE based on the mathematically consistent d_{30}-formulation instead of the classical mean droplet diameter. Yet another computationally cheap alternative is the interfacial area transport equation (IATE) method [85, 37] which considers the gas-liquid specific surface area as one of the most important parameters and it is based on the solution of the corresponding transport equation (for the interfacial area). The effect of bubble coalescence, due to the random turbulent collisions between bubbles, and of the wake entrainment process, due to the relative motions of the bubbles, can be accounted for. As far as bubble breakup is concerned instead the impact of turbulent eddies is considered. A similar method was also developed in [43, 44].

In this work, we present a new fast multiphase computational model for turbulent gas-liquid bubbly flows accounting for polydispersity. The unknown gas convection velocity is modelled by 1) employing the slip velocity method or 2) solving an ordinary differential equation. This equation resembles the E-L method, but the actual Lagrangian particle tracking is removed to achieve computational efficiency. It also resembles the Eulerian quadrature-based moments methods (E-QBMM), in which the velocity is modelled by the velocity polynomial assumption [58]. For these reasons we call this computational model the Quasi-Eulerian-Eulerian (Q-E-E) method. The first "Eulerian" denotes that the gas bubbles are convected by a single transport equation under the Eulerian framework, the second "Eulerian" denotes that the liquid phase continuity and momentum balance equations are employed. An additional transport equation was included to address bubble coalescence and breakage. The fluid phase equations and the additional transport equation for bubble coalescence and breakage are coupled by the drag force. We then validate the model predictions by comparison with predictions and experiments obtained in two classical gas-liquid bubble columns and one relatively new airlift column reported in the literature. To the author's best knowledge this method, although quite straightforward, was never published before nor implemented nor validated. It is eventually worth mentioning that the model has been implemented in OpenFOAM and is available for download and use. OpenFOAM-based simulation frameworks offer numerous advantages, including flexibility and ease uptake by the scientific community [9].

The remainder of the manuscript is as follows: in Section 2, the governing equations and numerical discretization of the Q-E-E method are discussed. The solver development and implementation are also described. In Section 3 and 4, the Q-E-E method solver is validated against three test cases. Finally, conclusions are drawn in Section 5.

2. Governing equations

The multiphase system is composed by different phases. It is common to assume the liquid phase as continuous phase and model it under the Eulerian framework [5]. In this manner, without taking into account for mass transfer, the mass conservation equation for the incompressible liquid phase (continuous phase) is described by the following continuity equation:

$$\frac{\partial \alpha_{\mathrm{c}}}{\partial t} + \nabla \cdot (\alpha_{\mathrm{c}} \mathbf{U}_{\mathrm{c}}) = 0 \tag{1}$$

where α_{c} is the phase fraction of the liquid phase and $\mathbf{U}_{\mathrm{c}}$ is its velocity. The momentum conservation of the liquid phase can be described by the volume-averaged incompressible momentum balance equation:

$$\rho_{\mathrm{c}} \frac{\partial (\alpha_{\mathrm{c}} \mathbf{U}_{\mathrm{c}})}{\partial t} + \rho_{\mathrm{c}} \nabla \cdot (\alpha_{\mathrm{c}} \mathbf{U}_{\mathrm{c}} \otimes \mathbf{U}_{\mathrm{c}}) = -\alpha_{\mathrm{c}} \nabla p + \alpha_{\mathrm{c}} \nabla \cdot \tau_{\mathrm{c}} + \alpha_{\mathrm{c}} \mathbf{g} - \mathbf{M}, \tag{2}$$

where p is the average pressure, ρ_{c} is the density, $\mathbf{g}$ is the gravity acceleration vector and $\mathbf{M}$ is the momentum interface exchange term to account for the momentum exchange between the gas phase and liquid phase, which will be discussed in the next section. τ_{c} represents the stress tensor, which can be calculated by:

$$\tau_{\mathrm{c}} = \mu_{\mathrm{c}} \left[\nabla \mathbf{U}_{\mathrm{c}} + (\nabla \mathbf{U}_{\mathrm{c}})^{\mathrm{T}} \right] - \frac{2}{3} \mu_{\mathrm{c}} (\nabla \cdot \mathbf{U}_{\mathrm{c}}) \mathbf{I} - \frac{2}{3} \rho k \mathbf{I}. \tag{3}$$

where k is the turbulent kinetic energy. Equation (1) and (2) are employed in the E-L, E-E and E-QBMM to predict the liquid phase flow field.

For the gas phase, it is quite common to address it as a disperse phase. The disperse phase can be modelled with different procedures. In the Lagrangian framework, the position and velocity of the bubbles can be computed by solving the force balance over the individual bubbles:

$$\frac{\mathrm{d}\mathbf{X}}{\mathrm{d}t} = \mathbf{V}_{\mathrm{d}}, \tag{4}$$

$$m_{\mathrm{d}} \frac{\mathrm{d}\mathbf{V}_{\mathrm{d}}}{\mathrm{d}t} = \mathbf{F}, \tag{5}$$

where $\mathbf{X}$ is the position vector, $\mathbf{V}_{\mathrm{d}}$ is the individual bubble velocity, m_{d} is the bubble mass, and $\mathbf{F}$ is the force exerted on discrete bubbles, which requires a certain degree of modelling. Here we assume that the bubble mass is constant and that there is no net momentum exchange due to mass transfer. Among the many relevant fluid-bubble interaction forces, the most important is produced by the stresses of the continuous phase on the bubble surface, resulting in the drag and buoyancy forces. The balance of these forces determines the terminal bubble velocity. The bubble phase fraction (α_{d}) and liquid phase fraction (α_{c}) can be updated by using the following equations:

$$\alpha_{\mathrm{d}} = \frac{\sum V_{\mathrm{d}}}{V_{\mathrm{cell}}}, \alpha_{\mathrm{c}} = 1 - \alpha_{\mathrm{d}}, \tag{6}$$

where V_{d} is the single bubble volume in a cell and V_{cell} is the cell volume.

The gas phase can be also modelled in the Eulerian framework resulting in equations similar to Eq. (1) and Eq. (2):

$$\frac{\partial \alpha_{\mathrm{d}}}{\partial t} + \nabla \cdot (\alpha_{\mathrm{d}} \mathbf{U}_{\mathrm{d}}) = 0 \tag{7}$$

where α_{d} is the phase fraction of the gas phase and $\mathbf{U}_{\mathrm{d}}$ is the average gas bubble velocity. The

momentum conservation can be described by the volume-averaged incompressible momentum balance equation:

$$\rho_{\mathrm{d}}\frac{\partial(\alpha_{\mathrm{d}}\mathbf{U}_{\mathrm{d}})}{\partial t}+\rho_{\mathrm{d}}\nabla\cdot(\alpha_{\mathrm{d}}\mathbf{U}_{\mathrm{d}}\otimes\mathbf{U}_{\mathrm{d}})=-\alpha_{\mathrm{d}}\nabla p+\nabla\cdot\tau_{\mathrm{d}}+\alpha_{\mathrm{d}}\mathbf{g}+\mathbf{M}, \tag{8}$$

where ρ_{d} is the density and τ_{d} represents the stress tensor.

On the other hand, one can also use the generalized population balance equation for the gas phase, which can be written as follows [58]:

$$\frac{\partial f}{\partial t}+\nabla_{\mathbf{X}}\cdot(\mathbf{U}_{\mathrm{d}}f)+\nabla_{\mathbf{U}_{\mathrm{d}}}\cdot(\mathbf{A}f)=\mathcal{S}, \tag{9}$$

where f is the number density function for the gas phase phase, characterizing the number of bubbles per unit volume with a certain velocity and size, $\mathcal{S}$ is the breakage and coalescence source term, $\mathbf{A}$ is the acceleration term, which is given by:

$$\mathbf{A}=-\frac{1}{\rho_{\mathrm{d}}}\nabla p+\mathbf{g}+\frac{1}{\rho_{\mathrm{d}}}\mathbf{M}. \tag{10}$$

The solution of Eq. (9) is usually achieved in terms the moments of the number density function and the corresponding closure problem is usually overcome by using a quadrature approximation.

Equation (4) and Eq. (5) can be solved via a meshless method by updating the Lagrangian bubble location without any numerical problems. Equations (1) - (6) constitute the set of equations employed in any E-L method. In the E-L method, numerical problems arise and need special treatments. For example, the phase fraction is a strictly bounded value ($0 \leqslant \alpha_{\mathrm{d}} < 1$). It should be smaller than one otherwise a vacuum state of the liquid phase can occur in certain cells. This also explains the reason why the bubble size should be smaller than the cell size and why a two-dimensional E-L simulation is not strictly applicable. Meanwhile, the bubble location tracking algorithm should be highly efficient otherwise the whole algorithm would be quite slow. It is suggested to employ the face penetrating method to locate the bubble location, but it sometimes fails and the bubble disappears if the bubble moves just through the cell vertices instead of the cell faces [19]. Equations (1), (2), (7) and (8) constitute the equations typically employed in the E-E method. The resulting transport equations are quite complex and difficult to solve. Depending on the source terms, its mathematical features also change and the employed numerical schemes should be consistent. Equations (1), (2) and (9) constitute the equations employed in the E-QBMM. This equation system is not closed and sub-models are necessary. Moreover, it is not trivial to maintain the realizability of the moments if a high-order scheme is used [72, 45, 66].

2.1. Gas phase velocity formulation

The governing equations employed in the Q-E-E method can be derived from the existing method using justifiable approximations. It can be seen from Eq. (1) and Eq. (2) that once the phase fraction α_{d} is calculated, they can be used to solve for the continuous phase velocity $\mathbf{U}_{\mathrm{c}}$ and pressure p. In the E-E method, α_{d} is convected by Eq. (7), in which $\mathbf{U}_{\mathrm{d}}$ is unknown. In the E-QBMM, the unknown $\mathbf{U}_{\mathrm{d}}$ is calculated from the moments, this method was also called the velocity-polynomial-approximation (VPA) method. On the other hand, considering a stagnant liquid environment ($\mathbf{U}_{\mathrm{c}}=0$), it was proven that the balance between the buoyancy force and the drag force can be achieved. Eventually, the bubble will ascent at a nearly constant velocity, namely the so-called terminal velocity. The force balance equation can be written as follows:

$$\rho_{\mathrm{d}}V_{\mathrm{d}}\mathbf{g}\left(1-\frac{\rho_{\mathrm{c}}}{\rho_{\mathrm{d}}}\right)=\frac{3}{4}C_D\frac{\rho_{\mathrm{c}}}{d}|\mathbf{U}_{\mathrm{d}}|\mathbf{U}_{\mathrm{d}}V_{\mathrm{d}}, \tag{11}$$

where V_d is the volume of single bubble, d is the bubble diameter, and C_D is the drag coefficient which requires a certain degree of modelling and different models were proposed. For example, in the Schiller and Naumann model, it can be calculated as follows:

$$C_D = \begin{cases} 24\left(1 + 0.15\mathrm{Re}^{0.687}\right)/\mathrm{Re}, & \mathrm{Re} \leqslant 1000, \\ 0.44, & \mathrm{Re} > 1000, \end{cases} \tag{12}$$

where Re is the Reynolds number defined by:

$$\mathrm{Re} = \frac{\rho_\mathrm{c} d|\mathbf{U}_\mathrm{c} - \mathbf{U}_\mathrm{d}|}{\mu_\mathrm{c}}, \tag{13}$$

where μ_c is the viscosity of the liquid phase. Substituting Eq. (12) into Eq. (11), the bubble terminal velocity can be calculated. Simulations showed that the bubble terminal velocity and the drag coefficient are strongly dependent on the bubble diameter under turbulent conditions [76, 81]. For air bubbles in clean water with size ranging from 3 mm to 5 mm, the bubble terminal velocity is approximately constant and equal to 0.23 m/s. If the Reynolds number is larger than 2000, C_D ranges from approximately 0.3 to 3 as measured in experiments. Therefore, it is safe to calculate the bubble velocity from the following equation:

$$\mathbf{U}_\mathrm{d} = \mathbf{U}_\mathrm{c} + \mathbf{U}_s, \tag{14}$$

where $\mathbf{U}_s$ is the slip velocity. This slip velocity assumption was also used in the mixture/drift-flux model. A similar approximation was also employed in other works and the justification was proven by several authors [5, 26]. In this work, we adopt a similar approach and we assume a constant slip velocity due to the reason that the bubble terminal velocity typically ranges only from 0.2 m/s to 0.25 m/s. A similar procedure was also adopted in other works [77]. In this manner, the gas phase velocity can be calculated and the capability of this method is investigated in this work. This is the first procedure investigated in this work.

Besides Eq. (14), an iterative procedure can be used to obtain the gas phase velocity, which is more consistent with the theory. In the field of E-L and E-QBMM, the gas phase velocity can be updated with the following ordinary differential equation (ODE):

$$\frac{\mathrm{d}\mathbf{U}_\mathrm{d}}{\mathrm{d}t} = \mathbf{g} - \frac{1}{\rho_\mathrm{d}}\nabla p_\mathrm{c} + \frac{1}{\tau}\left(\mathbf{U}_\mathrm{c} - \mathbf{U}_\mathrm{d}\right), \tag{15}$$

where τ is the relaxation time. Substituting the Bernoulli equation:

$$\nabla p_\mathrm{c} = \rho_\mathrm{c}\mathbf{g} \tag{16}$$

into Eq. (15) leads to:

$$\frac{\mathrm{d}\mathbf{U}_\mathrm{d}}{\mathrm{d}t} = \mathbf{g}\left(1 - \frac{\rho_\mathrm{c}}{\rho_\mathrm{d}}\right) + \frac{1}{\tau}\left(\mathbf{U}_\mathrm{c} - \mathbf{U}_\mathrm{d}\right). \tag{17}$$

When the Euler-implicit time scheme is employed to solve Eq. (17), the velocities for the next time step can be written as follows:

$$\mathbf{U}_\mathrm{d}^{t+\Delta t} = \frac{\mathbf{U}_\mathrm{d}^{t} + \Delta t\left(S_p\mathbf{U}_\mathrm{c} + S_u\right)}{1.0 + S_p\Delta t}, \tag{18}$$

where

$$
\begin{aligned}
S_u &= \mathbf{g}\left(\frac{\rho_\mathrm{d}-\rho_\mathrm{c}}{\rho_\mathrm{d}}\right), \\
S_p &= \frac{3}{4}\frac{\mu_\mathrm{c}}{\rho_\mathrm{d} d^2} C_D \mathrm{Re}.
\end{aligned} \tag{19}
$$

Since Eq. (19) depends on Re, which is in turn depends on $\mathbf{U}_\mathrm{d}$, an iterative procedure should be adopted. In practise, Eq. (19) can be solved 5 - 10 times to obtain a convergent gas phase velocity. Since no differential equation is evolved, the iterative procedure is quite fast and can be easily implemented. In this manner, the gas phase velocity can be obtained without assigning the value of the slip velocity. It should be noted here that other momentum interfacial exchange terms (e.g., lift force) can be included in S_u as reported in Eq. (19) and the solving procedure is straightforward. This is the second procedure investigated in this work.

Another problem that arises is how to model the bubble path dispersion. It is well known that the width of the rising bubble swarm increases with the height of the column. Thus, radial mixing takes place in the gas phase. But this effect cannot be properly represented because only a convective term exists in the gas phase transport equation. Under turbulent flow conditions, Eq. (7) should be averaged and the following equation can be obtained:

$$
\frac{\partial \alpha_\mathrm{d}}{\partial t} + \nabla \cdot (\alpha_\mathrm{d} \mathbf{U}_\mathrm{d}) + \nabla \cdot \left(\overline{\alpha'_\mathrm{d} \mathbf{U}'_\mathrm{d}}\right) = 0, \tag{20}
$$

where $\overline{\alpha'_\mathrm{d} \mathbf{U}'_\mathrm{d}}$ needs to be modelled and the overline represents the Reynolds averged employed in the context of the Reynolds-averaged Navier-Stokes equation (RANS) approach. The last term on the left-hand side of Eq. (20) justifies the use of a turbulent diffusion term in the phase transport equation. In this work, we adopted the approach extensively employed in the field of slurry simulations [18, 61]. In this model, the turbulent dispersion term was modelled by the following assumption:

$$
\nabla \cdot \left(\overline{\alpha'_\mathrm{d} \mathbf{U}'_\mathrm{d}}\right) = -\nabla \cdot \left(\frac{\nu_t}{\sigma} \nabla \alpha\right), \tag{21}
$$

where ν_t is the turbulent kinematic viscosity of the liquid phase, determined in turn by turbulence model and σ is the turbulent Schmidt number for gas bubble phase fraction. The turbulent Schmidt number may be interpreted as the ratio of turbulent momentum transport to the turbulent transport of the mass associated to the gas phase. However, its numerical value is not well established in the literature because no single constant value can be used. In the proposed model, we simply set the turbulent Schmidt number for volume fractions equal to 1.0, since this value results in the best overall agreement with the experimental data. The turbulent kinematic viscosity of the liquid can be calculated from the turbulence model. In this work, the standard $k-\varepsilon$ model was employed, which can be written as follows:

$$
\frac{\partial \varepsilon}{\partial t} + \nabla \cdot (\mathbf{U}\varepsilon) - \nabla \cdot (D_\varepsilon \nabla \varepsilon) = C_1 G \frac{\varepsilon}{k} - \frac{2}{3} C_1 \varepsilon \nabla \cdot \mathbf{U} - C_2 \frac{\varepsilon}{k}\varepsilon, \tag{22}
$$

$$
\frac{\partial k}{\partial t} + \nabla \cdot (\mathbf{U}k) - \nabla \cdot (D_k \nabla k) = G - \frac{2}{3}\nabla \cdot \mathbf{U}k - \varepsilon, \tag{23}
$$

where

$$
G = \nu_t \left(\nabla \mathbf{U} + \nabla \mathbf{U}^T - \frac{2}{3}(\nabla \cdot \mathbf{U})\mathbf{I}\right) : \nabla \mathbf{U}. \tag{24}
$$

Once the k and ε equation was solved, the turbulent viscosity can be calculated by

$$\nu_t = C_\mu \frac{k^2}{\epsilon}. \tag{25}$$

2.2. Bubble coalescence and breakage

To account for bubble breakage and coalescence, another model is needed. QMOM or EQMOM were implemented in our previous works but they are not suitable for this work due to the large demand of computational resources [52, 51, 49]. Therefore, we adopted a simpler procedure as reported in [43, 44]. In this method, the total bubble number density, n, equivalent to the moment of order zero of the bubble size distribution, is employed to calculate the local mean bubble size, d, as follows:

$$d = \left(\frac{\alpha_\mathrm{d}}{\pi/6n} \right)^{\frac{1}{3}}. \tag{26}$$

An additional transport equation is solved for n, accounting for the transport of bubbles (by convection and turbulent diffusion) and changes in bubble size (and therefore bubble number density) by breakage and coalescence [43, 44]:

$$\frac{\partial n}{\partial t} + \nabla \cdot (\mathbf{U}_\mathrm{d} n) - \nabla \cdot (\nu_t \nabla n) = S_\mathrm{break} - S_\mathrm{coal}, \tag{27}$$

where S_break is the source term to account for bubble breakage and S_coal is the sink term to account for bubble coalescence. It is important to stress here that with this simplified approach no direct information on the bubble size distribution is collected nor employed. Polydispersity is account for in the model only via Eq. (27) describing the effect that coalescence and breakage have on the local mean bubble size. The Q-E-E method is therefore capable of describing that the local mean bubble size changes from point to point and from a time instant to another in the reactor, but not that bubbles of different size can coexist in the same region of the reactor. R3.2 R3.3 R3.2

Some breakage kernels are derived from the Hinze theory that identifies the size of smallest bubble, namely the Hinze scale, which can be efficiently broken-up by turbulent eddies [33]. This characteristic size can vary depending on the fluid properties and surface tension from 1 mm (i.e. bubbles in ocean waves) to a few micrometers (i.e. liquid droplets in stirred tanks). Further studies in this area highlighted that, depending on the flow features, the bubble size distribution can follow a power-law scaling with different slopes. For bubbles larger than the Hinze scale, it shows for example a $-10/3$ exponent, with the smallest bubbles stabilized by the surface tension [84]. Studies focusing on bubble columns and bubbly flows confined in small pipe showed instead that the bubble size distribution follows a log-normal distribution. These findings have been used as validation rules in many works, especially those in which the bubble size distribution is directly described in the model, as for example in our previous work. However, this is not possible here, since as already mentioned, only Eq. (27) is solved and therefore only the local mean bubble size is known. R3.3

The rate of bubble breakage is assumed here to be related to the collision rate with turbulent eddies of similar size, since larger eddies merely transport the bubbles and smaller eddies have insufficient energy. The collision rate with eddies depends on the turbulent velocity, for which the bubble size is assumed to lie within the inertial sub-range of turbulence. Additionally, break-up is conditional on exceeding a critical value of bubble Weber number, We_c, representing the ratio of turbulent shear forces to the restoring surface tension forces. In this work we assume $\mathrm{We}_c = 0.5$. Following these

considerations, the expression for the break-up is assumed to be [43, 44, 85]:

$$S_{\text{break}} = C_{\text{br}} \frac{U_t}{1.4d} \sqrt{1.0 - \frac{-\text{We}_c}{\text{We}}} \exp\left(\frac{-\text{We}_c}{\text{We}}\right), \text{We} > \text{We}_c, \tag{28}$$

where C_{br} is an empirical coefficient, equal to 0.075, and U_t is taken to be the velocity of eddies in the inertial sub-range of the turbulent eddy spectrum, which may be written as:

$$U_t = 1.4(\varepsilon d)^{1/3}. \tag{29}$$

The bubble Weber number defines the tendency for bubbles to break up or remain stable, which can be written as:

$$\text{We} = \frac{\rho_{\text{c}} U_t d}{\sigma}, \tag{30}$$

where σ is the surface tension beween the gas and liquid phases. Bubble coalescence can be modelled by the random collision process or the wake induced collision process. In this work, we consider random collision, though the wake induced collision can be included straightforwardly. In the theory of random collision, the bubble coalescence sink term can be written as [43, 44, 85]

$$S_{\text{coal}} = n^2 C_{\text{turb}} U_t \frac{d^2}{\alpha_{\text{max}}^{1/3} \alpha_{\text{d}}^{1/3}} \left(1 - \exp\left(-C_{\text{turb2}} \frac{\alpha_{\text{max}}^{1/3} \alpha_{\text{d}}^{1/3}}{\alpha_{\text{max}}^{1/3} \alpha_{\text{d}}^{1/3} - \alpha_{\text{max}}^{1/3} \alpha_{\text{d}}^{1/3}}\right)\right), \tag{31}$$

where $C_{\text{turb}}, C_{\text{turb2}}$ are empirical coefficients equal to 0.05 and 0.75, respectively, and α_{max} is the maximum packing limit for the bubbles.

Eq. (20), Eq. (14), Eq. (1), Eq. (2) together with the equations of the turbulent model Eq. (22), Eq. (23) and the bubble diameter equation Eq. (27) form the governing equations of the Q-E-E method, which is suitable for polydisperse turbulent bubbly flows. It can be solved in the same way as in the single phase flow by some iterative procedure under the finite volume method, which will be discussed in the next section.

2.3. Numerical discretization

In this section, we summarise the iterative solving procedure based on the PISO algorithm [38]. The solving procedure of the Q-E-E method resembles the procedure of the E-QBMM and the E–L method. The spirit of the PISO algorithm is to use the momentum to obtain a non-divergence free velocity field, then use the continuity equation to construct a pressure Poisson equation to update the velocity field to ensure divergence free. The pressure equation is suggested to be solved 2 - 3 times within a time step. Special numerical techniques are necessary to prevent oscillations, especially when there are gradient terms and large body forces in the source term of the momentum equation.

In order to obtain a smooth solution, the pressure term (gradient term), gravity term and others are neglected at this step and the discretized form of Eq. (2) can be written as follows:

$$a_P \mathbf{U}_P + \sum a_N \mathbf{U}_N = S_P, \tag{32}$$

where a_P is the matrix diagonal coefficients, a_N is the matrix non-diagonal coefficients, $\mathbf{U}_P$ is the unknown velocity defined at the cell center, and $\mathbf{U}_N$ is the known velocity for the cell neighbours. The subscript $_{\text{d}}$ was neglected for brevity. Eq. (32) constitutes a matrix system which can be solved by any sparse linear system to obtain the predicted velocity. However, in practise, it is not solved and this step can be safely replaced by a one step Jacobian point iterative procedure. The solution

of this one step iterative procedure produces the predicted velocity:

$$\mathbf{HbyA}_P = \frac{-\sum a_N \mathbf{U}_N + S_P}{a_P}. \tag{33}$$

Due to the crude approximation, **HbyA** is meaningless and needs to be corrected. The convergent velocity and pressure should obey the continuity equation. The discretized continuity equation can be written as

$$\frac{(\alpha_{\mathrm{c},P}^{t+\Delta t} - \alpha_{\mathrm{c},P}^{t})\Delta V_P}{\Delta t} + \sum \left(\alpha_{\mathrm{c},f} \mathbf{U}_f^{t+\Delta t} \cdot \mathbf{S}_f\right) = 0, \tag{34}$$

where Δt is the time step, and ΔV_P is the cell volume. Owing to the Rhie and Chow interpolation, the cell face velocity can be expressed by [69]

$$\mathbf{U}_f^{t+\Delta t} = \mathbf{HbyA}_f - \frac{1}{a_P}\alpha_{\mathrm{c},f}(\nabla p)_f + \alpha_{\mathrm{c},f}\frac{1}{a_P}\mathbf{g} - \frac{1}{a_P}\mathbf{M}_f. \tag{35}$$

Substituting Eq. (35) into Eq. (34) leads to

$$\sum \frac{\alpha_{\mathrm{c},f}^2}{a_P}(\nabla p)_f = \frac{(\alpha_{\mathrm{c},P}^{t+\Delta t} - \alpha_{\mathrm{c},P}^{t})\Delta V_P}{\Delta t} + \sum \left(\alpha_{\mathrm{c},f}\left(\mathbf{HbyA}_f + \frac{\alpha_{\mathrm{c},f}}{a_P}\mathbf{g} - \frac{1}{a_P}\mathbf{M}_f\right) \cdot \mathbf{S}_f\right). \tag{36}$$

The continuous form of Eq. (36) is the so-called pressure Poisson equation and its solution gives the pressure of the continuous phase. It should be noted here that the term associated with **g** is the gravity/buoyancy term and the term associated with **M** is the momentum exchange interfacial term. In some works, it was claimed that the effect of the buoyancy term is larger than that of the momentum exchange term. In this work, the effect of the buoyancy term was evaluated. In summary, the solving procedure consists of the following steps:

1. From the initial field, calculate the momentum exchange term and construct the velocity matrix system as reported in Eq. (32); Calculate the predicted velocity as reported in Eq. (33) by the one point Jacobian method;
2. Solve the pressure Poisson equation as reported in Eq. (36) to update pressure.
3. Reconstruct the velocity from the pressure as reported in Eq. (35). Repeat step 2 and 3 two or three times and a convergent velocity/pressure field of the continuous phase can be obtained.
4. Update the dispersed phase velocity by using Eq. (14) (i.e. constant slip or procedure 1) or Eq. (18) (i.e. ODE or procedure 2) and calculated the phase transported equation as reported in Eq. (20). Update the continuous phase fraction by $\alpha_{\mathrm{c}} = 1 - \alpha_{\mathrm{d}}$.
5. Correct the turbulence equations and bubble size equation and move to the next time step.

The implementation of the algorithm mentioned previously is straightforward and it is briefly discussed here. The velocity matrix system can be constructed by:

```
fvVectorMatrix UcEqn
(
    fvm::ddt(alphac, Uc) + fvm::div(alphaPhic, Uc)
  - fvm::Sp(fvc::ddt(alphac) + fvc::div(alphaPhic), Uc)
  + continuousPhaseTurbulence->divDevRhoReff(Uc)
 ==
  - fvm::Sp(dragSp, Uc)
);
```

in which the drag force was discretized semi-implicitly. The predicted velocity **HbyA** can be solved by

```
HbyA = UEqn.H()/UEqn.A();
```

The face velocity of the continuous phase as reported in Eq. (35) can be implemented by

```
Kd = 0.75*alphad*muc/sqr(diameter)*CdRe;
preDispersed = Kd*Ud;
surfaceScalarField phicForces
(
    fvc::flux(rAUc*preDispersed/rhoc)
  - (
      fvc::interpolate(rAUc*(Su)) & mesh.Sf()
    )
  + alphacf*rAUcf*(g & mesh.Sf())
);
surfaceScalarField phiHbyA
(
    "phiHbyA",
    (
       fvc::flux(HbyA)
     + alphacf*rAUcf*fvc::ddtCorr(Uc, phic)
     + phicForces
    )
);
```

where `CdRe` is $C_D\mathrm{Re}$. Afterwards, the pressure Poisson equation can be implemented by

```
fvScalarMatrix pEqn
(
    fvm::laplacian(sqr(alphacf)*rAUcf, p)
 ==
    fvc::ddt(alphac) + fvc::div(alphacf*phiHbyA)
);
```

and the velocity can be reconstructed by

```
Uc = HbyA
  + rAUc*fvc::reconstruct((phicForces - pEqn.flux()/alphacf)/rAUcf);
```

All the governing equations are implemented in the open-source CFD code OpenFOAM and wrapped into a new solver called `QEEFoam`. In this work, the code and test cases are open-sourced. Readers are referred to the supplementary files for download.

3. Test cases and numerical details

The predicted results obtained with the `QEEFoam` are compared with the measurements available in the literature both for qualitative and quantitative comparisons. The first test case (Test A) simulated in this work is a partially aerated rectangle bubble column investigated by Becker et al. [7]. The second test case (Test B) is a rectangle bubble column investigated by Díaz et al. [23]. The third test case (Test C) is an airlift bubble column investigated by Mandalahalli et al. [56]. The first two cases are characterised by a simple geometry with a complicated flow structure, which are suitable for numerical investigation. Depending on the experimental conditions, the flow regimes resulting from time/volume-averaged procedures can differ considerably from the unsteady flow structures. The fully developed vortex flow has been proved to be a very useful tool to evaluate the hydrodynamic properties of bubble columns. The last test case is rather new and the geometry is quite different from the previous two. It could be a good test case for further validation.

The column was filled with tap water (i.e. continuous liquid phase) at room temperature and atmospheric pressure, while the air was fed through an aluminium sparger. A sketch of the setup

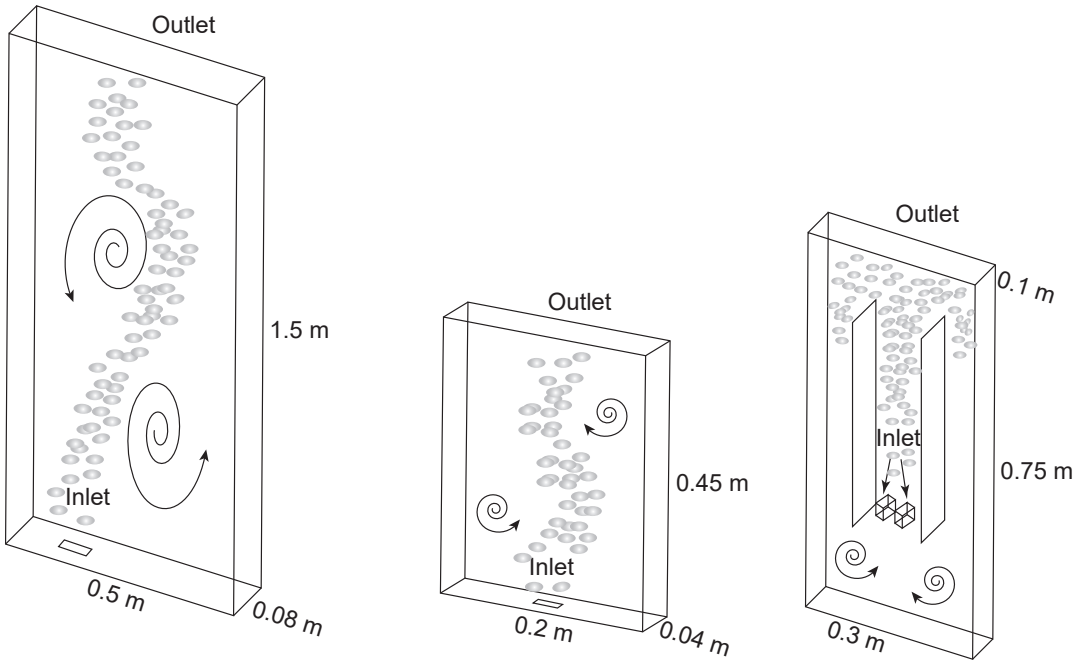

Figure 1: Bubble column geometry investigated experimentally by Becker et al. (left) [7], Díaz et al. (middle) [23]. Airlift column geometry investigated experimentally by Mandalahalli et al. (right) [56].

is shown in Fig. 1. A fully orthogonal hexahedral grid measuring 52 (height) × 32 (width) × 18 (depth) cells for test A and 40 (height) × 21 (width) × 9 (depth) cells for test B were generated by `blockMesh` utility, as we confirmed that these non-uniform hexahedral grids are enough to capture the plume oscillations in our previous investigations. A similar mesh resolution was also reported in other works [23, 47, 64, 62]. The sparger inlet, generated by `topoSet` and `createPatch` utilities, through which the gas bubbles enter the domain was modelled as a rectangle with an area equal to 0.001197 m^2 and 0.00021 m^2, respectively. This simplification has been proven to be efficient for meshing, and previous works have shown that the results are not sensitive to the inlet shape [23, 13]. For test case C, a non-uniform hexahedral grid was employed. The diameter of bubbles in test A, B and C is 3 mm, 5.05 mm and 2.2 mm, respectively. Different gas superficial velocities were used and will be reported in the following sections. The buoyancy force, drag force and the turbulent dispersion force were considered in all the test cases in the Q-E-E simulations. Second order with a limiter convection scheme was used for all variables. In our test cases, the unbounded problem of the phase fraction and bubble number density was not shown.

Some results were also compared with that predicted by the OpenFOAM E-L solver `DPMFoam`. In the E-L simulations, rebounded wall boundary and "escape" boundary were given for the bubbles. The bubble number injected per second to the computational domain was calculated from the superficial gas velocity as

$$n = \frac{\mathbf{U}_s \mathbf{S}_{\text{outlet}}}{V_{\text{bubble}}}, \tag{37}$$

where n the bubble number injected per second, $\mathbf{S}_{\text{outlet}}$ is the surface vector, $\mathbf{U}_s$ is the gas superficial velocity, and V_{bubble} is the bubble volume. Sizes of the bubble were assumed to be uniform. Bubble collision is not considered and therefore a two-way coupling was assumed. In all the simulations, the liquid phase was assumed to be stagnant at the beginning. The non-slip velocity boundary condition

was given for the liquid velocity. For the liquid pressure, a zero gradient with the hydrodynamic correction was applied. The standard turbulent wall function was applied for turbulent variables.

As previously mentioned two algorithms are tested for the calculation of the gas bubble velocity:

1. by assuming a constant gas-liquid slip velocity and by using Eq. (14),
2. by updating the gas bubble velocity with the solution of the ODE discretized in Eq. (18).

4. Results and discussions

4.1. Test case A

In this test case the gas was injected on the left side of the bottom. One can certainly expect that vortices may exist due to the non-symmetric injection. It was also shown in previous works that the dynamic liquid circulation is quite complex and can only by predicted by three-dimensional simulations [62, 77]. Therefore, our algorithm and implementation should capture such quasi-periodic transient liquid circulations. The predicted and measured horizontal liquid velocities for test case A at different positions with slip velocity method and ODE method are reported in Fig. 2 and table 1. It can be seen that the quasi-periodic transient liquid circulations are successfully captured. The horizontal liquid velocity at point A is slightly larger than that predicted for point B since point A is located at the left side, which is in good agreement with what has been reported in the literature [7, 77]. The effect of the turbulent dispersion term on the period of bubble plum oscillation (POP) is negligible (within 10 %) as it is seen in table 1. Meanwhile, it can be found that the user-defined slip velocity has a substantial effect on the POP. A larger slip velocity corresponds to large relative velocity and the coupling between the gas and liquid phase is stronger, which implies a small relaxation time and smaller POP. It was also shown that a vertical slip of 0.2 m/s predicted the best results compared with the experimental data. Such slip velocity value agrees well with the experimental founding as mentioned in section 2. On the other hand, the ODE method predicts quite good POP as well, since the gas phase velocity was predicted by solving the ODE system and the user-defined slip velocity is not necessary.

	With dispersion term	Without dispersion term
Slip vel. method 0.15 m/s	54 s	53 s
Slip vel. method 0.2 m/s	40 s	37.5 s
Slip vel. method 0.25 m/s	35 s	30 s
ODE method	39 s	37 s

Table 1: Comparison of predicted and experimentally measured POP for the test case A with/without turbulent dispersion term. Different vertical slip velocity were used. Measured POP: 41 s.

The prediction of the oscillating phase fraction, velocity, and streamlines coloured by pressure at different time instants ($\Delta t = 2$ s) for the test case A by the slip velocity method are reported in Fig. 3. Results predicted by the ODE method is not shown for brevity since the difference is negligible. They show a surprisingly good agreement with experiments. Several liquid circulation cells can be observed in the column, typically no more than 4 circulation zones can be found. The vortex at the top tends to increases its size. When the upper vortex reaches a critical size, it starts to move downwards. The size of the largest vortex is as large as half of the column. Once these large vortices reached the bottom, they are smeared due to the wall and new vortices are generated at the top. At this point, the "cycle" is repeated again. Meanwhile, the center of the vortex has a relatively low pressure, which is consistent with the vortex theory. It can be seen that such a dynamic vortex

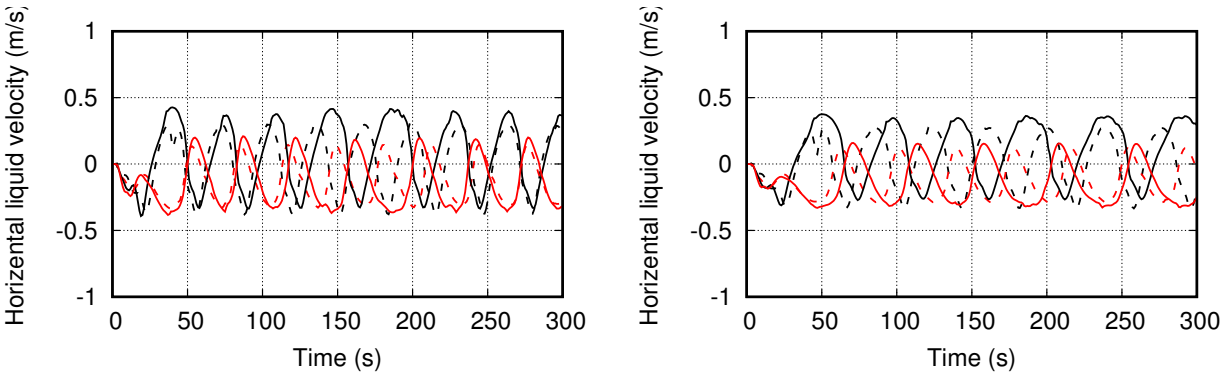

(a) Slip velocity method, $\mathbf{U}_y = 0.25$ m/s

(b) Slip velocity method, $\mathbf{U}_y = 0.2$ m/s

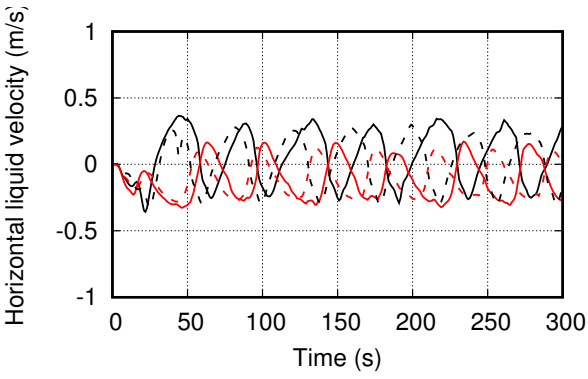

(c) ODE method

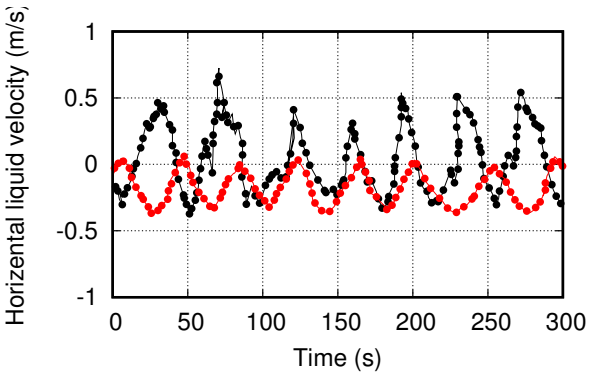

(d) Experimental data

Figure 2: Calculated horizontal liquid velocities for test case A at different positions by the slip velocity method and ODE method. Black line: (0.035 0.9 0.04), red line: (0.45 1.05 0.04). Solid line: with turbulent dispersion term. Dashed line: without turbulent dispersion term.

movement can be surprisingly captured by our code. On the other hand, the transient phase fraction shows similar oscillating plumes. After the gas was injected from the bottom, it was dispersed by the turbulent dispersion term and moved forward due to buoyancy. The time-averaged vertical liquid velocity predicted by the slip velocity method and the ODE method at different positions are reported in Fig. 4. The results predicted by the ODE method seem to be more accurate than those predicted by the slip velocity method, that tend to result in overpredictions (for slip velocity 0.25 m/s) or underpredictions (for slip velocity 0.15 m/s). When the slip velocity was fixed equal to 0.2 m/s good agreement with experimental results [7, 77] was observed. This test case shows that the flow field can be successfully predicted by the slip velocity method and the ODE method, where the results may be influenced by the user-defined slip velocity and a fitting procedure may be necessary for the first one. All these results show that our method is capable of predicting the turbulent bubbly plume.

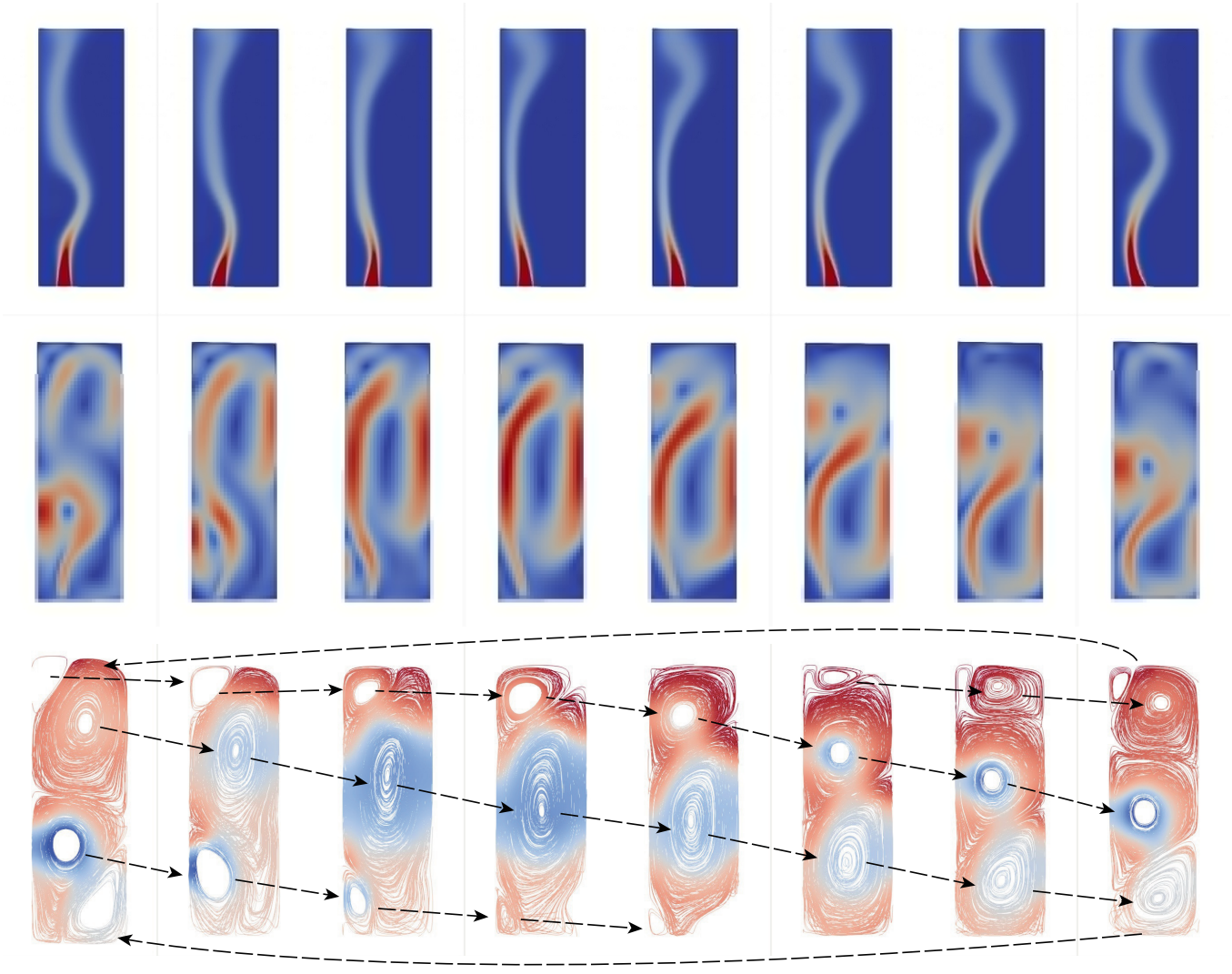

Figure 3: Prediction of the oscillating phase fraction (top, [0:0.03]), velocity (middle, [0:0.4]), and streamlines (bottom, colored by pressure, [-0.07:0.04]) at different time instants ($\Delta t = 2$ s) for test case A.

4.2. Test case B

In this test case, the gas was injected in the middle of the bottom, which implies the geometry is quite symmetric. Nonetheless, it was also shown in previous works that the dynamic liquid circulation

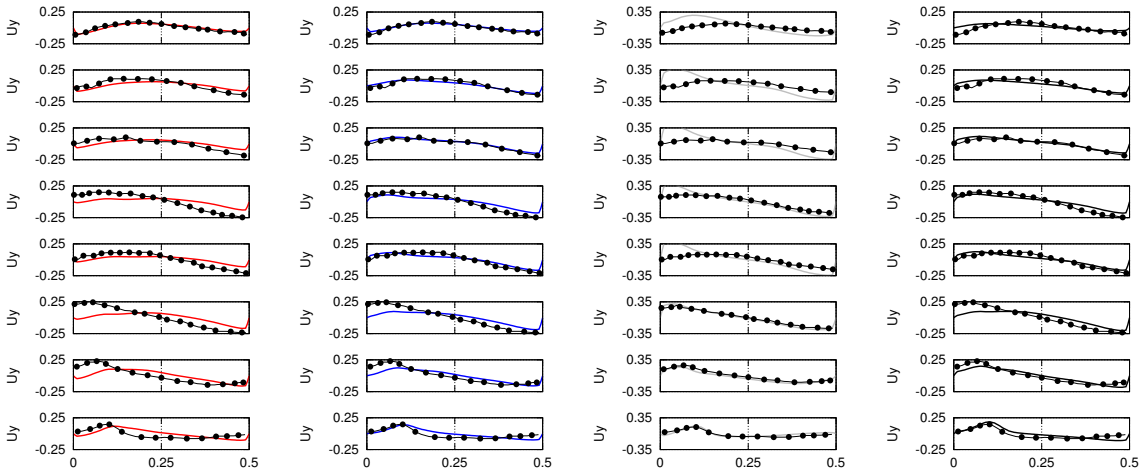

(a) Slip U is 0.15 m/s (b) Slip U is 0.2 m/s (c) Slip U is 0.25 m/s (d) ODE method

Figure 4: Comparison of the time-averaged upward liquid velocity with experimental data (points) at different heights on the mid-depth plane (from bottom to top: $y/H = 0.11, 0.22, 0.35, 0.49, 0.6, 0.7, 0.78, 0.89$).

is quite complex, as also confirmed by experiments [23]. In the experiments, different gas superficial velocities were employed. The predicted horizontal liquid velocity at different positions is reported in Fig. 5. The drag model developed by Grace et al. was employed [32]. Since the slip velocity method was investigated in the previous case, in this teat case, the magnitude of the slip velocity was assumed to be 0.25 m/s. Specifically, the predicted values of the gas POP are reported in table 2. It can be seen that the results predicted by the Q-E-E method agree well with the simulated results reported in the literature [23] and our previous works [47, 52, 13] in which the E-E and E-QBMM were used to simulate bubbly flows. In particular, the POP predicted by the slip velocity method is comparable with that predicted by the ODE method, which implies that a slip velocity of 0.25 m/s is suitable for this test case. It should be noted here that a 0.2 m/s slip velocity seems to be better for the previous case. This slip velocity acts as a tuning parameter in our method and a fitting procedure is required.

The predicted gas POP when the superficial velocity is 0.012 m/s with and without the gravity term exerted on the continuous phase is reported in Fig. 6. It can be seen that the predicted gas POP with or without the gravity term differs within 5%. Meanwhile, it was found that the momentum interfacial exchange term effect is very important, which implies that the coupling of the gas and liquid phases by the momentum transfer is also quite important. Similar predictions were also obtained with the E-L simulations solved by `DPMFoam`, which are not shown here for brevity. Such finding may contradict with others where the phase coupling was seen as more important than the momentum coupling. The prediction of the oscillating phase fraction and time-averaged phase fraction with and without turbulent dispersion term are reported in Fig. 7. It is obvious that the predicted gas phase fraction is quite sharp if the turbulent dispersion term is neglected in the transport equation, which is consistent with the theory. With the turbulent dispersion force bubbles spread deeper into the column. If one compares the predicted transient phase fraction with the experiments, it is also obvious that the predicted results with turbulent dispersion term are more accurate.

The time-averaged gas hold-up and vertical liquid velocity at different positions with and without turbulent dispersion term are reported in Fig. 8. Here the gas superficial velocity is 0.012 m/s. Different drag coefficients were employed and only the results predicted by the slip velocity method are reported. Predictions obtained by the E-L method are also used as a comparison. It can be seen

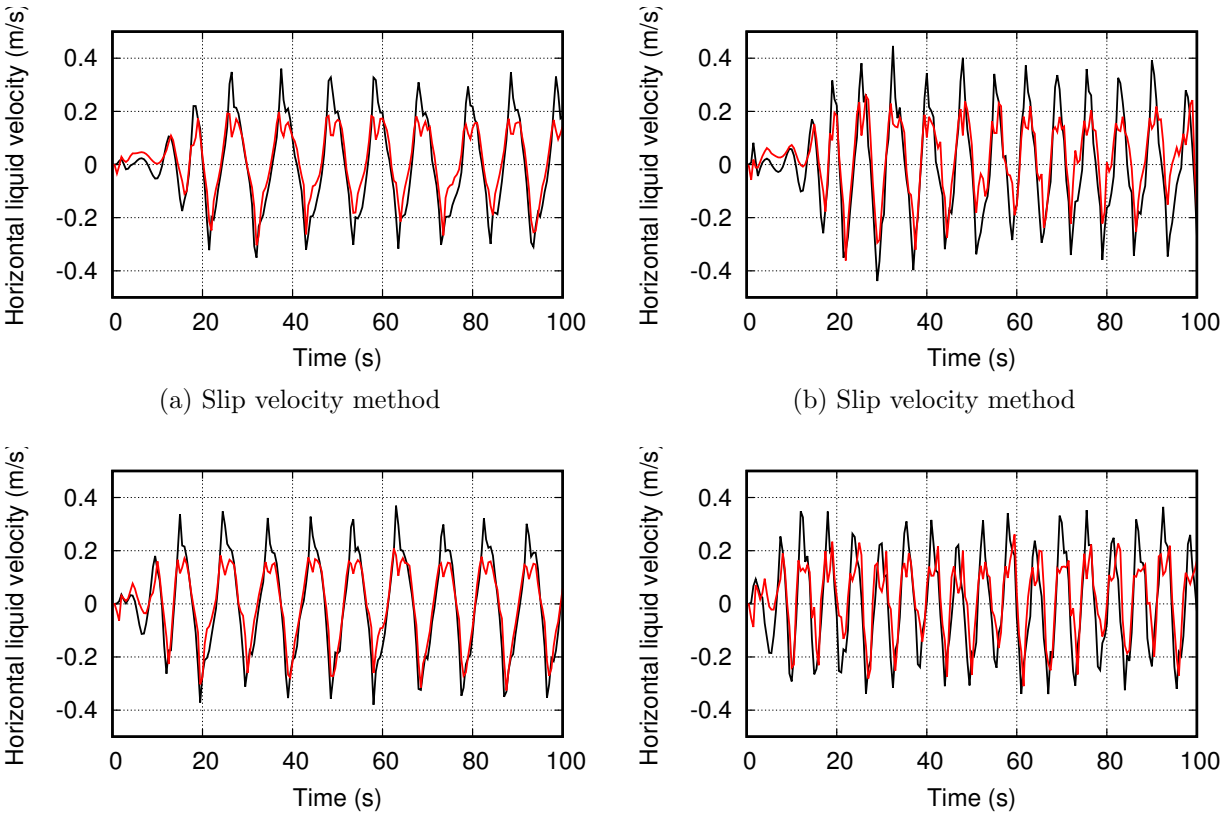

(a) Slip velocity method

(b) Slip velocity method

(c) ODE method

(d) ODE method

Figure 5: Calculated horizontal liquid velocity for test case B operated at different superficial gas velocities (left: 0.0024 m/s, right: 0.0071 m/s) at different positions (black line: x = 0.1 m, y = 0.225 m, z = 0.02 m; red line: x = 0.05 m, y = 0.225 m, z = 0.02 m) by slip velocity method ($|\mathbf{U}_s| = 0.25$ m/s) and ODE method.

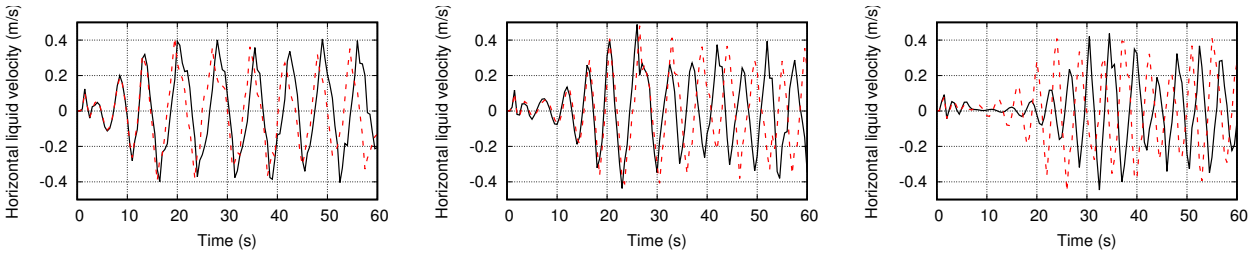

(a) SchillerNaumann drag model

(b) Grace drag model

(c) Tomiyama drag model

Figure 6: Calculated horizontal liquid velocity for test case B operated with (black solid line) or without (red dashed line) gravity term by the slip velocity method. Different drag models were employed. Position: x = 0.1 m, y = 0.225 m, z = 0.02 m. The superficial gas velocity is 0.012 m/s.

Gas superficial velocity	Experiments	Predictions by slip vel.	Predictions by ODE
0.0024 m/s	11.37 s	11.5 s	11.4 s
0.0071 m/s	5.69 s	6.3 s	5.45 s
0.012 m/s	4.3 s	4.9 s	4.1 s

Table 2: Comparison of predicted and experimentally measured POP for the test case B with turbulent dispersion term by the slip velocity method and ODE method.

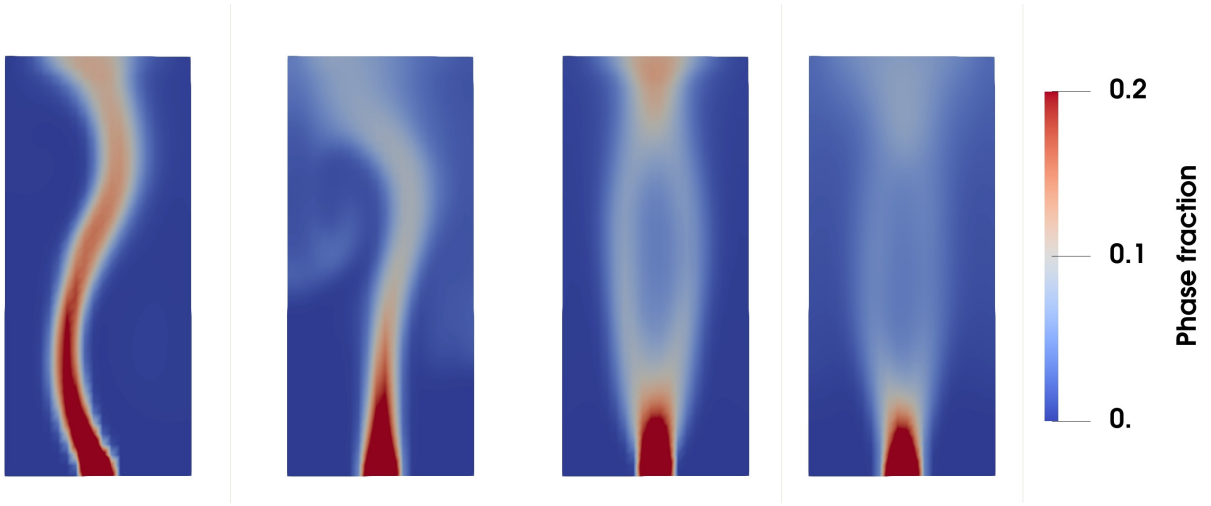

Figure 7: Prediction of the oscillating phase fraction and time-averaged phase fraction with and without turbulent dispersion term by the ODE method.

that the phase fraction predicted without the turbulent dispersion term shows an over-estimated double peak, which can be also seen in Fig. 7. This double peak comes from the periodic oscillating flow fields. On the other hand, results predicted with the turbulent dispersion term by the Q-E-E method agree well with those predicted by the E-L method. The drag model also has an effect on the predictions but the effect can be neglected. The predicted vertical liquid velocities by the Q-E-E method also agree well with that predicted by the E-L method. It can be observed that the resulting time-averaged flow pattern consists of a non-uniform velocity distribution presenting an upward flow in the column center and a downward flow along the column walls, a liquid circulation mode. This type of flow differs considerably from the instantaneous flow pattern previously described. The calculated global gas hold-up by the Q-E-E method at different superficial gas velocities is reported in Fig. 9. It can be seen that the predictions agree well with the experiments. All these results reveal that the dynamic vortex flow fields in a symmetric geometry can be predicted by the Q-E-E method and the results are surprisingly good. The prediction of the bubble size distribution of test case B with different gas superficial velocities was reported in Fig. 10. It can be seen that the mean bubble size is larger at the center of the column than at the sides. Contour plots of the mean bubble size show that, with the increase of the gas superficial velocity, smaller bubbles tend to stay in the liquid recirculation path, whereas bigger bubbles are concentrated into the central plume zone where coalescence and breakup occur with faster rates due to turbulence. Such results were also observed in other works where a QBMM was used [11].

4.3. Test case C

The feature of test case C is that it is a new test case and the geometry is quite complex. The Q-E-E method should be able to predict accurate results no matter what the geometry is. The time-averaged gas hold-up at different positions with different gas superficial velocities are reported in Fig. 11. It is seen that the profile of the time-averaged local gas fraction above the sparger plate ($z = 0.25$ m) shows an expected M-shape profile, which was also observed in the experiments. The peaks correspond to the gas fraction at the centers of the spargers. With increasing the superficial velocity, there is an increase in the overall number of bubbles and thus an increased gas fraction. The turbulent dispersion effect was negligible, since the bubbles were just injected into the column and the flow was not fully developed. For the middle section ($z = 0.35$ m), the effect of the turbulent

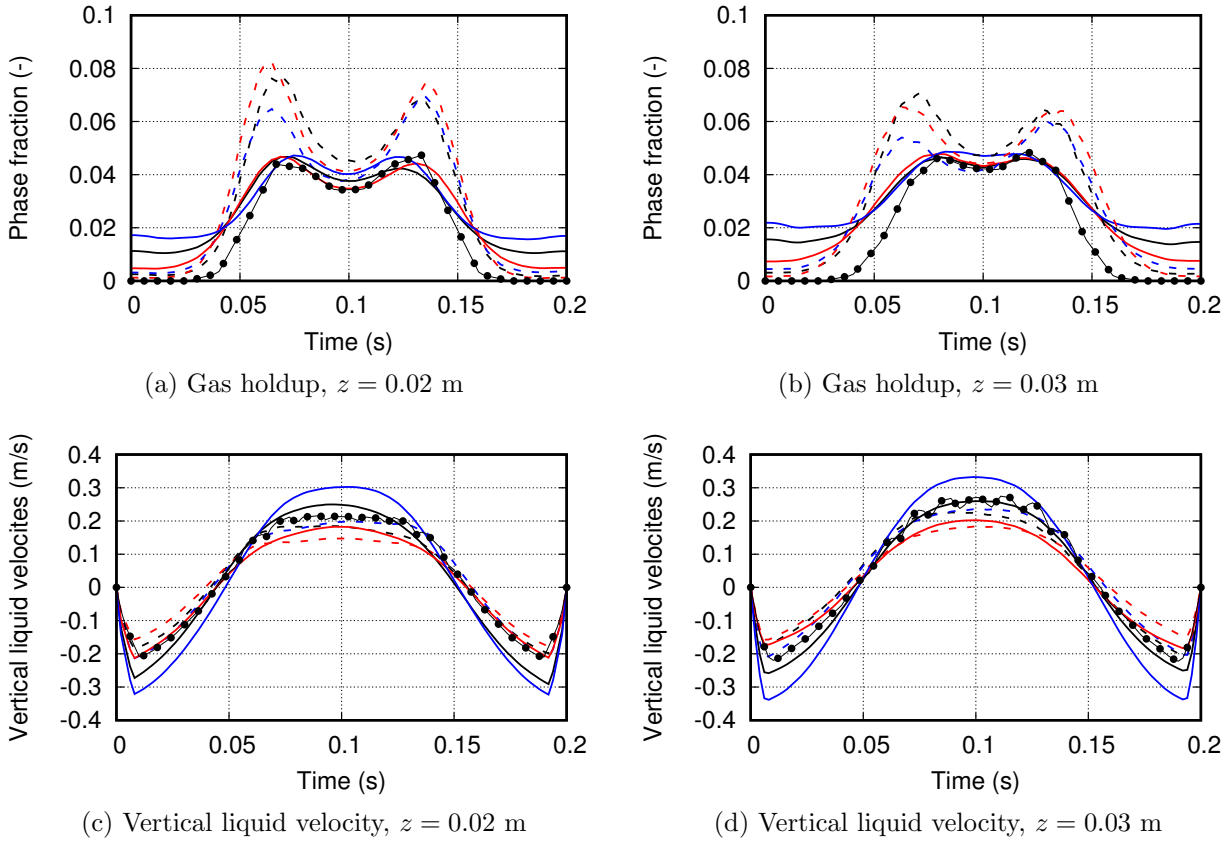

(a) Gas holdup, $z = 0.02$ m

(b) Gas holdup, $z = 0.03$ m

(c) Vertical liquid velocity, $z = 0.02$ m

(d) Vertical liquid velocity, $z = 0.03$ m

Figure 8: Time-averaged gas hold-up and vertical liquid velocity at different positions for test Case B. Gas superficial velocity is 0.012 m/s. Different drag coefficients were employed. Solid line: with turbulent dispersion term. Dashed line: without turbulent dispersion term by the slip velocity model. Black: Grace drag model, red: SchillerNaumann drag model, blue: Tomiyama drag model. Black line-points: data simulated by E-L method with SchillerNaumann drag model.

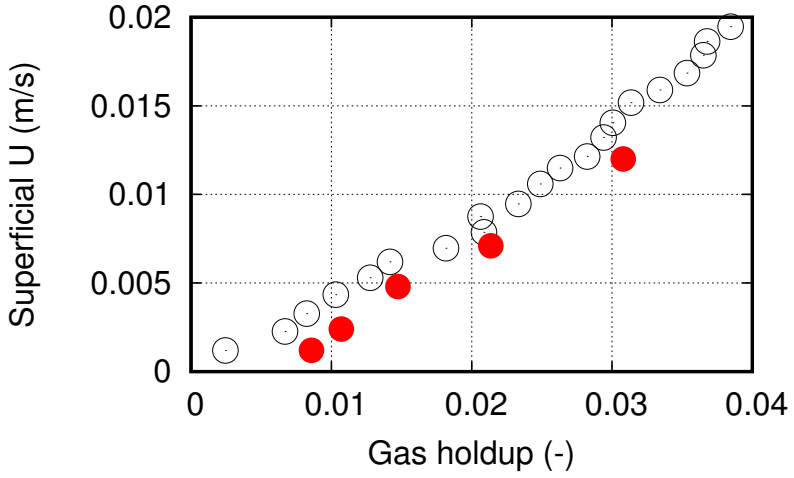

Figure 9: Comparison between experimental (black circles) and calculated global gas hold-up (red circles) at different superficial gas velocities for test case B slip velocity method.

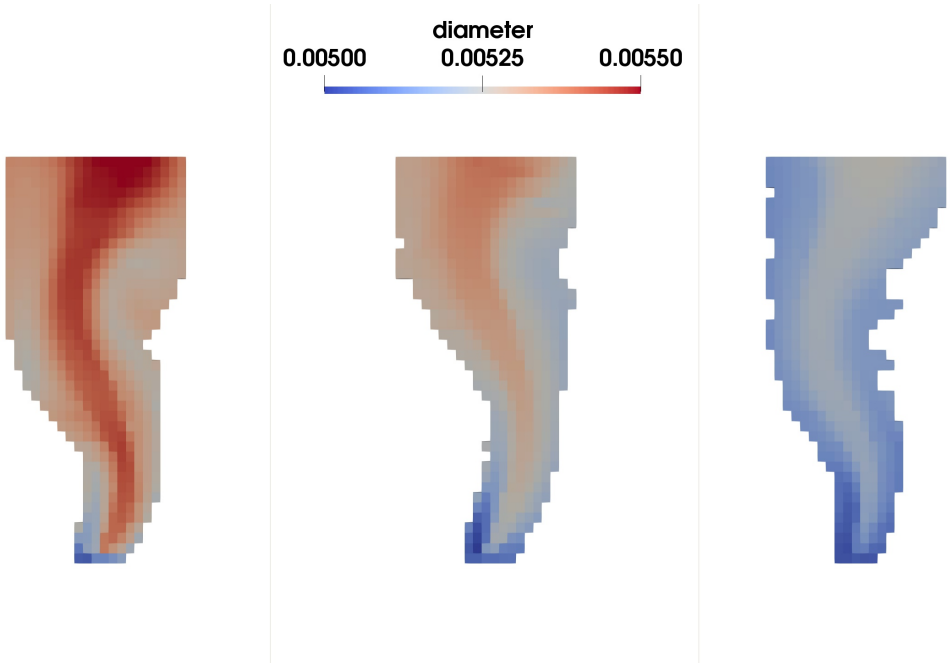

Figure 10: Prediction of the bubble size distribution of test case B with different gas superficial velocity (left: 0.012 m/s, middle: 0.0071 m/s, right: 0.0024 m/s).

dispersion cannot be omitted and it can be seen that the phase fraction can be only predicted accurately when the turbulent dispersion was included, otherwise a over-estimated double peak was predicted. The predicted phase fraction at the upper riser section was underestimated ($z = 0.58$ m). Improvements can be obtained by selecting other drag models or by fitting the bubble breakage and coalescence parameters. Meanwhile, the polydisperse predictions showed a significant difference with monodisperse results for high gas superficial velocity (0.0032 m/s). The difference of the results between monodisperse and polydisperse predictions for small gas superficial velocity is negligible. This can be explained by the fact that bubble breakage and coalescence is not frequent for these operating conditions. On the other hand, the difference of the results between monodisperse and polydisperse predictions for large gas superficial velocity is notable. This was also observed in test case B since the bubble coalescence and breakage are dominant for flows operated under larger superficial gas velocities.

At last we assess the computational efficiency by comparing the running CPU times of the OpenFOAM original two-fluid solver `reactingTwoPhaseEulerFoam` and `QEEFoam`. The comparison is reported in Fig. 12 ($\Delta t = 0.01$ s). All the simulations were launched by one CPU processor (Intel i7-5820K).

5. Conclusions

In this work, a fast Eulerian-based approach which is suitable for polydisperse turbulent gas-liquid flow was proposed and implemented in the open-source CFD code OpenFOAM-7 as `QEEFoam`. This method solves only one set of Navier-Stokes equations for the liquid phase. The gas phase was transported under the Eulerian framework by a convection equation. Turbulent effects can be included by adding a turbulent dispersion term in the gas phase equation.

The unknown gas phase velocity is calculated by:

1. assuming a constant slip velocity between the gas bubble and the surrounding liquid phase

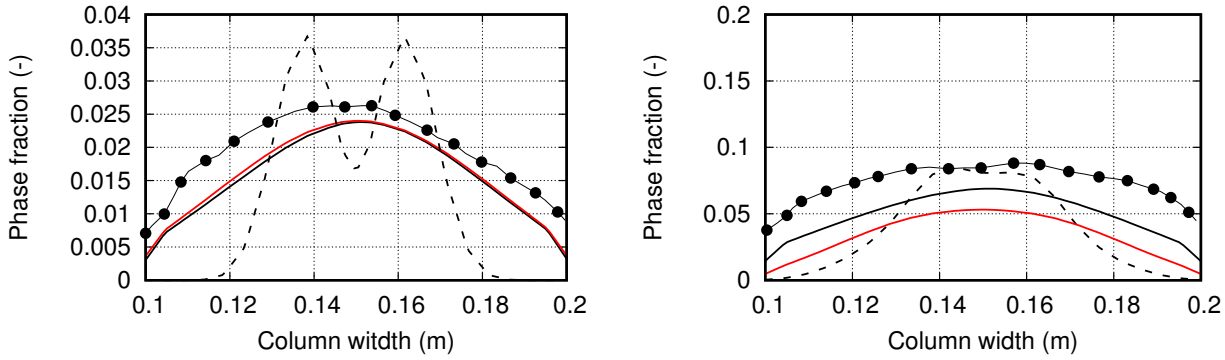

(a) $z = 0.58$ m

(b) $z = 0.58$ m

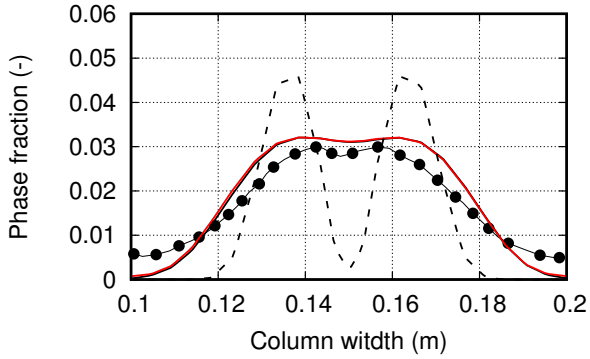

(c) $z = 0.35$ m

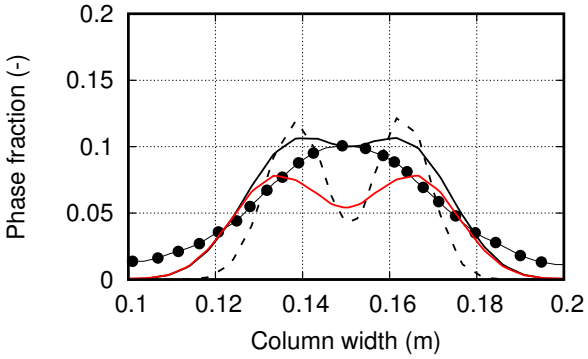

(d) $z = 0.35$ m

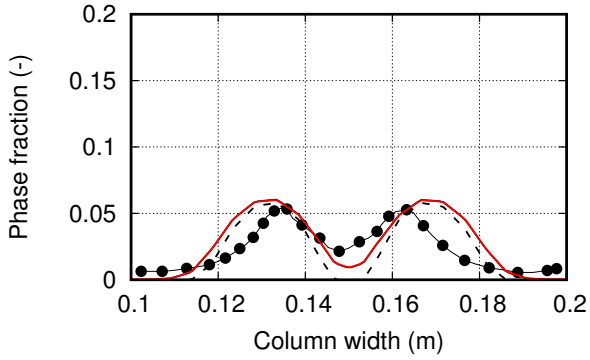

(e) $z = 0.25$ m

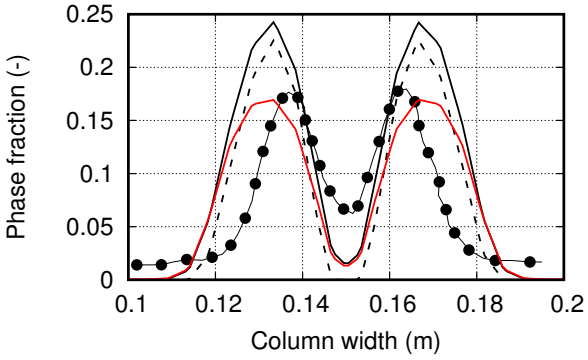

(f) $z = 0.25$ m

Figure 11: Time-averaged gas hold-up at different positions by the ODE method for test case C. Gas superficial velocity is 0.008 m/s (left) and 0.032 m/s (right). Solid line: with turbulent dispersion term. Dashed line: without turbulent dispersion term. Line-points: experimental data. Black: monodisperse. Red: polydisperse.

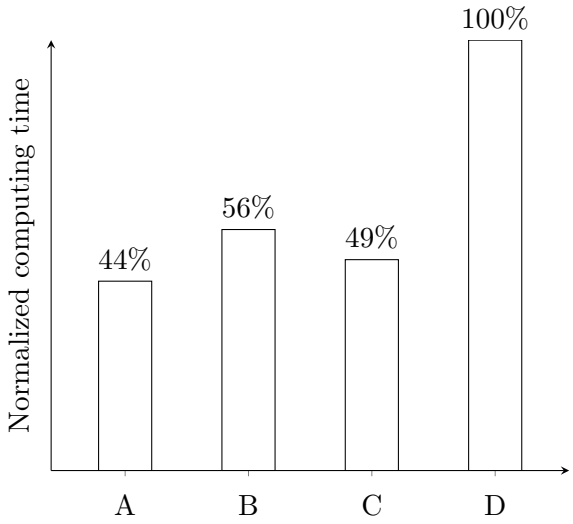

Figure 12: Comparison of the computing efficiency between `QEEFoam` and `reactingTwoPhaseEulerFoam` for test case B. A: monodisperse `QEEFoam` (slip vel. method, 327 s). B: monodisperse `QEEFoam` (ODE method, 413 s). C: polydisperse `QEEFoam` (slip vel. method, 362 s). D: monodisperse `reactingTwoPhaseEulerFoam` (732 s).

2. solving an ODE for the gas bubble velocity which accounts for the interfacial forces acting on the bubble

A user-defined slip velocity is needed for the first method, while no empirical parameters are necessary for the second one. The bubble size is determined by including a transport equation for the total bubble number density. Bubble breakage and coalescence are modelled as source and sink terms. The whole equation system can be solved by any iterative solution procedure (e.g., PISO algorithm). Our algorithm and implementation are validated against three test cases characterized by different geometries and by different gas superficial velocities. The uncertainty associated with the constant slip velocity assumption and the effect of turbulent dispersion are assessed. The importance of the drag momentum exchange term is also assessed.

Predictions for the local/global gas phase fraction, period of oscillation the gas bubble plume and horizontal/vertical transient/time-averaged liquid velocity are compared with experimental data or simulation results predicted by the E-L method. Our results show that the methodology is capable of adequately describing very complex dynamic flow fields in the bubble columns. Good agreement between the predictions with experimental data can be obtained. The slip velocity method can predict comparable results with those predicted by the ODE system if a suitable slip velocity is chosen, with slightly smaller computational costs. Compared with the existing CFD-PBE coupling algorithm (e.g., QMOM or CM), `QEEFoam`, which solves for the total bubble number density transport equation, is stable and fast. In conclusion, our algorithm seems a very promising and fast strategy for the simulation of industrial polydisperse turbulent gas-liquid flow.

References

[1] DriftFluxFoam tutorial test case does not settle. https://bugs.openfoam.org/view.php?id=2317. Accessed: 2022-01-30.

[2] Z. Ahmed, D. Izbassarov, P. Costa, M. Muradoglu, and O. Tammisola. Turbulent bubbly channel flows: Effects of soluble surfactant and viscoelasticity. *Computers & Fluids*, 212:104717, 2020.

[3] M. Attarakih, M. Abu-Khader, and H. Bart. Modeling and dynamic analysis of a rotating disc contactor (RDC) extraction column using one primary and one secondary particle method (OPOSPM). *Chemical Engineering Science*, 91:180–196, 2013.

[4] M. Attarakih, A. Hasseine, and H. Bart. CFD modelling of bubbly gas flow using coupled OPOSPM-Two-Fluid Model. *Computer Aided Chemical Engineering*, 38:403–408, 2016.

[5] S. Balachandar and J.K. Eaton. Turbulent dispersed multiphase flow. *Annual Review of Fluid Mechanics*, 42:111–133, 2010.

[6] M. Banaei, N.G. Deen, M. van Sint Annaland, and J.A.M. Kuipers. Particle mixing rates using the two-fluid model. *Particuology*, 36:13–26, 2018.

[7] S. Becker, A. Sokolichin, and G. Eigenberger. Gas—liquid flow in bubble columns and loop reactors: Part II. Comparison of detailed experiments and flow simulations. *Chemical Engineering Science*, 49:5747–5762, 1994.

[8] C.E. Blenkinsopp and J.R. Chaplin. Bubble size measurements in breaking waves using optical fiber phase detection probes. *IEEE Journal of Oceanic Engineering*, 35:388–401, 2010.

[9] G. Boccardo, E. Crevacore, A. Passalacqua, and M. Icardi. Computational analysis of transport in three-dimensional heterogeneous materials: An openfoam-based simulation framework. *Computing and Visualization in Science*, 23(1-4), 2020.

[10] G. Boccardo, I.M. Sokolov, and A. Paster. An improved scheme for a robin boundary condition in discrete-time random walk algorithms. *Journal of Computational Physics*, 374:1152–1165, 2018.

[11] A. Buffo, D.L. Marchisio, M. Vanni, and P. Renze. Simulation of polydisperse multiphase systems using population balances and example application to bubbly flows. *Chemical Engineering Research and Design*, 91:1859–1875, 2013.

[12] A. Buffo, M. Vanni, and D. Marchisio. Simulation of a reacting gas–liquid bubbly flow with CFD and PBM: Validation with experiments. *Applied Mathematical Modelling*, 44:43–60, 2017.

[13] A. Buffo, M. Vanni, D.L. Marchisio, and R.O. Fox. Multivariate quadrature-based moments methods for turbulent polydisperse gas–liquid systems. *International Journal of Multiphase Flow*, 50:41–57, 2013.

[14] V.V. Buwa, D.S. Deo, and V.V. Ranade. Eulerian–lagrangian simulations of unsteady gas–liquid flows in bubble columns. *International Journal of Multiphase Flow*, 32:864–885, 2006.

[15] J. Capecelatro and O. Desjardins. An Euler–Lagrange strategy for simulating particle-laden flows. *Journal of Computational Physics*, 238:1–31, 2013.

[16] S. Castellano, N. Sheibat-Othman, D. Marchisio, A. Buffo, and S. Charton. Description of droplet coalescence and breakup in emulsions through a homogeneous population balance model. *Chemical Engineering Journal*, 354:1197–1207, 2018.

[17] E.G. Chatzi and C. Kiparissides. Drop size distributions in high holdup fraction dispersion systems: effect of the degree of hydrolysis of PVA stabilizer. *Chemical Engineering Science*, 49:5039–5052, 1994.

[18] X. Chen, Y. Li, X. Niu, M. Li, D. Chen, and X. Yu. A general two-phase turbulent flow model applied to the study of sediment transport in open channels. *International Journal of Multiphase Flow*, 37:1099–1108, 2011.

[19] R. Chorda, J.A. Blasco, and N. Fueyo. An efficient particle-locating algorithm for application in arbitrary 2D and 3D grids. *International Journal of Multiphase Flow*, 28:1565–1580, 2002.

[20] M. Colombo and M. Fairweather. Multiphase turbulence in bubbly flows: RANS simulations. *International Journal of Multiphase Flow*, 77:222–243, 2015.

[21] E. Crevacore, G. Boccardo, D.L. Marchisio, and R. Sethi. Microscale colloidal transport simulations for groundwater remediation. *Chemical Engineering Transactions*, 47:271–276, 2016. cited By 6.

[22] G.B. Deane and M. D. Stokes. Scale dependence of bubble creation mechanisms in breaking waves. *Nature*, 418:839–844, 2002.

[23] M.E. Díaz, A. Iranzo, D. Cuadra, R. Barbero, F.J. Montes, and M.A. Galán. Numerical simulation of the gas–liquid flow in a laboratory scale bubble column: influence of bubble size distribution and non-drag forces. *Chemical Engineering Journal*, 139:363–379, 2008.

[24] C. Drumm, M. Attarakih, M.W. Hlawitschka, and H. Bart. One-group reduced population balance model for CFD simulation of a pilot-plant extraction column. *Industrial & Engineering Chemistry Research*, 49:3442–3451, 2010.

[25] J. Ferry and S. Balachandar. A fast eulerian method for disperse two-phase flow. *International Journal of Multiphase Flow*, 27:1199–1226, 2001.

[26] J. Ferry and S. Balachandar. Equilibrium expansion for the eulerian velocity of small particles. *Powder Technology*, 125:131–139, 2002.

[27] J. Ferry, S.L. Rani, and S. Balachandar. A locally implicit improvement of the equilibrium eulerian method. *International Journal of Multiphase Flow*, 29:869–891, 2003.

[28] C. Garrett, M. Li, and D. Farmer. The connection between bubble size spectra and energy dissipation rates in the upper ocean. *Journal of Physical Oceanography*, 30:2163–2171, 2000.

[29] L. Gemello, V. Cappello, F. Augier, D. Marchisio, and C. Plais. CFD-based scale-up of hydrodynamics and mixing in bubble columns. *Chemical Engineering Research and Design*, 136:846–858, 2018.

[30] L. Gemello, C. Plais, F. Augier, A. Cloupet, and D. Marchisio. Hydrodynamics and bubble size in bubble columns: Effects of contaminants and spargers. *Chemical Engineering Science*, 184:93–102, 2018.

[31] L. Gemello, C. Plais, F. Augier, and D.L. Marchisio. Population balance modelling of bubble columns under the heterogeneous flow regime. *Chemical Engineering Journal*, 372:590–604, 2019.

[32] J.R. Grace, T. Wairegi, and T.H. Nguyen. Shapes and velocities of single drops and bubbles moving freely through immiscible liquids. *Chemical Engineering Research and Design*, 54:167–173, 1976.

[33] J.O. Hinze. Fundamentals of the hydrodynamic mechanism of splitting in dispersion processes. *AIChE Journal*, 1:289–295, 1955.

[34] M.T. Horsch, C. Niethammer, G. Boccardo, P. Carbone, S. Chiacchiera, M. Chiricotto, J.D. Elliott, V. Lobaskin, P. Neumann, P. Schiffels, M.A. Seaton, I.T. Todorov, J. Vrabec, and W.L. Cavalcanti. Semantic interoperability and characterization of data provenance in computational molecular engineering. *Journal of Chemical and Engineering Data*, 65(3):1313–1329, 2020.

[35] M. Icardi, G. Ronco, D. Marchisio, and M. Labois. Efficient simulation of gas–liquid pipe flows using a generalized population balance equation coupled with the algebraic slip model. *Applied Mathematical Modelling*, 38:4277–4290, 2014.

[36] M. Ishii and T. Hibiki. *Thermo-fluid dynamics of two-phase flow*. Springer Science & Business Media, 2010.

[37] M. Ishii and S. Kim. Development of one-group and two-group interfacial area transport equation. *Nuclear Science and Engineering*, 146:257–273, 2004.

[38] R.I. Issa, A.D. Gosman, and A.P. Watkins. The computation of compressible and incompressible recirculating flows by a non-iterative implicit scheme. *Journal of Computational Physics*, 62:66–82, 1986.

[39] D. Jain, J.A.M. Kuipers, and N.G. Deen. Numerical study of coalescence and breakup in a bubble column using a hybrid volume of fluid and discrete bubble model approach. *Chemical Engineering Science*, 119:134–146, 2014.

[40] H.A. Jakobsen, B.H. Sannæs, S. Grevskott, and H.F. Svendsen. Modeling of vertical bubble-driven flows. *Industrial & Engineering Chemistry Research*, 36:4052–4074, 1997.

[41] M. Karimi, H. Droghetti, and D.L Marchisio. PUfoam: A novel open-source CFD solver for the simulation of polyurethane foams. *Computer Physics Communications*, 217:138–148, 2017.

[42] S. Kumar and D. Ramkrishna. On the solution of population balance equations by discretization—I. A fixed pivot technique. *Chemical Engineering Science*, 51:1311–1332, 1996.

[43] G.L. Lane, M.P. Schwarz, and G.M. Evans. Predicting gas–liquid flow in a mechanically stirred tank. *Applied Mathematical Modelling*, 26:223–235, 2002.

[44] G.L. Lane, M.P. Schwarz, and G.M. Evans. Numerical modelling of gas–liquid flow in stirred tanks. *Chemical Engineering Science*, 60:2203–2214, 2005.

[45] F. Laurent and T.T. Nguyen. Realizable second-order finite-volume schemes for the advection of moment sets of the particle size distribution. *Journal of Computational Physics*, 337:309–338, 2017.

[46] D. Li, A. Buffo, W. Podgórska, D. Marchisio, and Z. Gao. Investigation of droplet breakup in liquid–liquid dispersions by CFD–PBM simulations: The influence of the surfactant type. *Chinese Journal of Chemical Engineering*, 25:1369–1380, 2017.

[47] D. Li and H. Christian. Simulation of bubbly flows with special numerical treatments of the semi-conservative and fully conservative two-fluid model. *Chemical Engineering Science*, 174:25–39, 2017.

[48] D. Li, Z. Gao, A. Buffo, W. Podgorska, and D. Marchisio. Droplet breakage and coalescence in liquid–liquid dispersions: Comparison of different kernels with EQMOM and QMOM. *AIChE Journal*, 63:2293–2311, 2017.

[49] D. Li, Z. Li, and Z. Gao. Compressibility induced bubble size variation in bubble column reactors: Simulations by the CFD–PBE. *Chinese Journal of Chemical Engineering*, 26(10):2009–2013, 2018.

[50] D. Li, Z. Li, and Z. Gao. Quadrature-based moment methods for the population balance equation: An algorithm review. *Chinese Journal of Chemical Engineering*, 27:483–500, 2019.

[51] D. Li, D. Marchisio, C. Hasse, and D. Lucas. Comparison of Eulerian QBMM and classical Eulerian–Eulerian method for the simulation of polydisperse bubbly flows. *AIChE Journal*, 65:e16732, 2019.

[52] D. Li, D. Marchisio, C. Hasse, and D. Lucas. twoWayGPBEFoam: An open-source Eulerian QBMM solver for monokinetic bubbly flows. *Computer Physics Communications*, page in press, 2019.

[53] M.R. Loewen, M.A. O'Dor, and M.G. Skafel. Bubbles entrained by mechanically generated breaking waves. *Journal of Geophysical Research: Oceans*, 101:20759–20769, 1996.

[54] M. Lopez De Bertodano, W. Fullmer, A. Clausse, and V. Ransom. *Two-Fluid Model Stability, Simulation and Chaos*. Springer, 2016.

[55] E. Madadi-Kandjani and A. Passalacqua. An extended quadrature-based moment method with log-normal kernel density functions. *Chemical Engineering Science*, 131:323–339, 2015.

[56] M.M. Mandalahalli, E.C. Wagner, L.M. Portela, and R.F. Mudde. Electrolyte effects on recirculating dense bubbly flow: An experimental study using X-ray imaging. *AIChE Journal*, 66:e16696, 2020.

[57] M. Manninen, V. Taivassalo, and S. Kallio. On the mixture model for multiphase flow. *VTT Publications 288*, Technical Research Center of Finland, 1996.

[58] D.L. Marchisio and R.O. Fox. *Computational models for polydisperse particulate and multiphase systems*. Cambridge University Press, 2013.

[59] R. McGraw. Description of aerosol dynamics by the quadrature method of moments. *Aerosol Science and Technology*, 27:255–265, 1997.

[60] X. Meng, X. Zhang, and Q. Li. Numerical investigation of nanofluid natural convection coupling with nanoparticles sedimentation. *Applied Thermal Engineering*, 95:411–420, 2016.

[61] G.V. Messa, M. Malin, and S. Malavasi. Numerical prediction of fully-suspended slurry flow in horizontal pipes. *Powder Technology*, 256:61–70, 2014.

[62] R.F. Mudde and O. Simonin. Two-and three-dimensional simulations of a bubble plume using a two-fluid model. *Chemical Engineering Science*, 54:5061–5069, 1999.

[63] B. Ničeno, M.T. Dhotre, and N.G. Deen. One-equation sub-grid scale (SGS) modelling for Euler–Euler large eddy simulation (EELES) of dispersed bubbly flow. *Chemical Engineering Science*, 63:3923–3931, 2008.

[64] R.S. Oey, R.F. Mudde, and H.E.A. Van den Akker. Sensitivity study on interfacial closure laws in two-fluid bubbly flow simulations. *AIChE Journal*, 49:1621–1636, 2003.

[65] A. Passalacqua and R.O. Fox. Implementation of an iterative solution procedure for multi-fluid gas–particle flow models on unstructured grids. *Powder Technology*, 213:174–187, 2011.

[66] A. Passalacqua, F. Laurent, and R.O. Fox. A second-order realizable scheme for moment advection on unstructured grids. *Computer Physics Communications*, 248:106993, 2020.

[67] W. Podgórska. *Multiphase Particulate Systems in Turbulent Flows: Fluid-liquid and Solid-liquid Dispersions*. CRC Press, 2019.

[68] A. Prosperetti and G. Tryggvason. *Computational methods for multiphase flow*. Cambridge university press, 2009.

[69] C.M. Rhie and W.L. Chow. Numerical study of the turbulent flow past an airfoil with trailing edge separation. *AIAA Journal*, 21:1525–1532, 1983.

[70] G. Rojas and M.R. Loewen. Fiber-optic probe measurements of void fraction and bubble size distributions beneath breaking waves. *Experiments in Fluids*, 43:895–906, 2007.

[71] Steffen Salenbauch, Christian Hasse, Marco Vanni, and Daniele L Marchisio. A numerically robust method of moments with number density function reconstruction and its application to soot formation, growth and oxidation. *Journal of Aerosol Science*, 128:34–49, 2019.

[72] M. Shiea, A. Buffo, M. Vanni, and D.L. Marchisio. A novel finite-volume TVD scheme to overcome non-realizability problem in quadrature-based moment methods. *Journal of Computational Physics*, page 109337, 2020.

[73] B. Shotorban and S. Balachandar. A Eulerian model for large-eddy simulation of concentration of particles with small stokes numbers. *Physics of Fluids*, 19:118107, 2007.

[74] B. Shotorban and S. Balachandar. Two-fluid approach for direct numerical simulation of particle-laden turbulent flows at small stokes numbers. *Physical Review E*, 79:056703, 2009.

[75] B.K. Singh, S. Roy, and V.V. Buwa. Bubbling/slugging flow behavior in a cylindrical fluidized bed: ECT measurements and two-fluid simulations. *Chemical Engineering Journal*, 383:123120, 2020.

[76] A. Sokolichin, G. Eigenberger, and A. Lapin. Simulation of buoyancy driven bubbly flow: established simplifications and open questions. *AIChE Journal*, 50:24–45, 2004.

[77] A. Sokolichin and G.S. Eigenberger. Applicability of the standard k–ε turbulence model to the dynamic simulation of bubble columns: Part I. detailed numerical simulations. *Chemical Engineering Science*, 54(13-14):2273–2284, 1999.

[78] G. Soligo, A. Roccon, and A. Soldati. Breakage, coalescence and size distribution of surfactant-laden droplets in turbulent flow. *Journal of Fluid Mechanics*, 881:244–282, 2019.

[79] S. Sundaresan, A. Ozel, and J. Kolehmainen. Toward constitutive models for momentum, species, and energy transport in gas–particle flows. *Annual Review of Chemical and Biomolecular Engineering*, 9:61–81, 2018.

[80] K. Swiderski, C. Narayanan, and D. Lakehal. Application of N-phase algebraic slip model and direct quadrature method of moments to the simulation of air-water flow in vertical risers and bubble column reactor. *Computers & Chemical Engineering*, 90:151–160, 2016.

[81] M. Talaia. Terminal velocity of a bubble rise in a liquid column. *World Academy of Science, Engineering and Technology*, 28:264–268, 2007.

[82] B.V. Tran, D. Nguyen, S. Ngo, Y. Lim, B. Kim, D. Lee, K. Go, and N. Nho. Hydrodynamics and simulation of air–water homogeneous bubble column under elevated pressure. *AIChE Journal*, 65:in press, 2019.

[83] A. Vaidheeswaran, W.D. Fullmer, and M. Lopez De Bertodano. Effect of collision force on well-posedness and stability of the two-fluid model for vertical bubbly flows. *Nuclear Science and Engineering*, 184:353–362, 2016.

[84] Z. Wang, J. Yang, and F. Stern. High-fidelity simulations of bubble, droplet and spray formation in breaking waves. *Journal of Fluid Mechanics*, 792:307–327, 2016.

[85] Q. Wu, S. Kim, M. Ishii, and S.G. Beus. One-group interfacial area transport in vertical bubbly flow. *International Journal of Heat and Mass Transfer*, 41:1103–1112, 1998.

[86] D. Zheng, W. Zou, C. Peng, Y. Fu, J. Yan, and F. Zhang. CFD-PBM coupled simulation of liquid-liquid dispersions in spray fluidized bed extractor: Comparison of three numerical methods. *International Journal of Chemical Engineering*, 2019:in press, 2019.

[87] T. Ziegenhein, A. Tomiyama, and D. Lucas. A new measuring concept to determine the lift force for distorted bubbles in low morton number system: Results for air/water. *International Journal of Multiphase Flow*, 108:11–24, 2018.